

AD-A258 569



2

The Development of the Navy's Multivariate Optimum Interpolation Analysis System

DTIC
ELECTE
DEC 09 1992
S E D

E. H. Barker
Prediction Systems Division
Atmospheric Directorate
Monterey, CA 93943-5006

92-31178



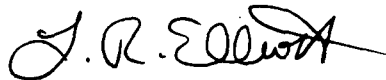
Approved for public release; distribution is unlimited. Naval Oceanographic and Atmospheric Research Laboratory, Stennis Space Center, Mississippi 39529-5004.

Foreword

The mathematical basis of the Navy's multivariate optimum interpolation (MVOI) analysis system is presented in detail. The analysis is used operationally to analyze data for the Operational Global Atmospheric Prediction System (NOGAPS 3), the Operational Regional Atmospheric Prediction System (NORAPS 5), and in the Navy's forecaster work station, the Tactical Environmental Support System (TESS (3)). The purpose of this document is to help Navy personnel to use the MVOI, and to serve as documentation of the analysis system.



W. B. Moseley
Technical Director



L. R. Elliott, Commander, USN
Officer in Charge

Executive Summary

The equations for the Navy's multivariate optimum interpolation (MVOI) analysis system for atmospheric analysis are presented in complete form. Included are the derivations for horizontal and vertical covariances that retain the geostrophic constraint and blend various kinds of observations such as pressure thickness, pressure height, and winds. Methods that scale the observation values to the resulting nondimensional values so that they are consistent with the constraints are presented.

The derivations of the analysis equations are provided using optimal theory to minimize the analysis error variance. The derivation of the internal data checking procedure is given. The method compares suspicious values with neighboring values and removes rejected values in a computationally consistent manner.

Validation experiments that show the exactness of the constraints, expected analysis error, and the method for analysis of wind around the poles are presented. These experiments have known results, and therefore are useful in catching design and program errors.

A brief description is provided of the observation selection procedures and internal quality control, and some recommendations for improvement are given.

Accession For	
NTIS	CRA&I <input checked="" type="checkbox"/>
DTIC	TAB <input type="checkbox"/>
Unannounced <input type="checkbox"/>	
Justification	
By	
Distribution /	
Availability Codes	
Dist	Avail and / or Special
A-1	

Acknowledgments

Dr. Jim Goerss applied the MVOI to the various applications at the Fleet Numerical Oceanography Center, Monterey, CA. Ms. Gail Brown Bayler wrote the quick-sort software used to process the observations for analysis. Prof. Richard Franke provided many helpful discussions during the development of the MVOI. Nancy Baker developed the observation data base and data quality control software. Also, thanks to Dr. John Hovermale for encouraging this work.

This research was supported by the Space and Naval Warfare Systems Command (PMW-165), under Program Element 0603207N, Capt. C. Hoffman, Program Manager.

The mention of commercial products or the use of company names does not in any way imply endorsement by the U.S. Navy or NOARL.

Contents

1.0 Introduction	1
2.0 Horizontal Covariances	2
3.0 Vertical Covariances	9
4.0 Variable Scaling	9
5.0 Optimizing the Analysis	11
6.0 Validation of Analysis System	18
7.0 Data Selection Procedures	28
8.0 Internal Quality Control	30
9.0 Conclusions	31
10.0 References	32

The Development of the Navy's Multivariate Optimum Interpolation Analysis System

1.0 Introduction

The Fleet Numerical Oceanography Center (FNOC) supports Navy Fleet operations. To be effective, the center has had to evolve into a numerical prediction center capable of support throughout the world. A key component of this support is the Navy Operational Global Atmospheric Prediction System (NOGAPS) described by Rosmond (1992) and Hogan and Rosmond (1991). Besides providing an analysis and prediction of weather patterns, it drives other predictions such as the Thermal Ocean Prediction System (TOPS), the Global Spectral Ocean Wave Model (GSOWM), and the Wave Model (WAM) with momentum and heat fluxes.

With continual increases in computer power and a wider diversity of observation platforms, a sophisticated analysis system was required to effectively assimilate data into NOGAPS. As a result, the multivariate optimum interpolation (MVOI) analysis was developed by the Naval Oceanographic and Atmospheric Research Laboratory (NOARL). This analysis method is similar to those developed at other centers such as the National Center for Atmospheric Research (NCAR) (Schlatter, 1975), the Canadian Atmospheric Environment Service (Rutherford, 1976, 1978), the National Meteorological Center (Bergman, 1976, 1979), and the European Center for Medium-Range Weather Forecasts (ECMWF) (Lorenc, 1981). Although optimum procedures have been known for over 30 years (Gandin, 1963), their potential was not fully realized until the 1980's when sufficiently powerful computers allowed the optimum interpolation software design to utilize hundreds of data values for each grid point rather than tens of values, more sophistication in the quality control procedures, and increased accuracy in determining the data and assimilation system error characteristics (see Barker and Rosmond, 1985). ECMWF exploited these options on their supercomputers, and many of their findings were included in the design and development of the Navy's system.

The Navy's MVOI became operational early in 1988 (Barker, et al., 1988) with the implementation of NOGAPS 3.0. The new system included upgrades in all components: the finite difference model was replaced by a spectral model, the calculus of variations initialization was replaced with the nonlinear normal mode method, and the successive corrections analysis was replaced with the MVOI.

This report provides the formulations and reasoning used in the development of the MVOI, and some of the validation experiments that also show functionality of the design options.

A major portion of the development of this system went into preparing the raw data for analysis. This involved pulling the raw data from the packed format in the FNOC data base, reformatting it, and then transferring

it into a data base on the supercomputer. Data quality control procedures are applied on the CYBER 205 data base as described in Baker (1991a-d). Rather than develop new tables for a new format, the one developed by the World Meteorological Organization for the Global Atmospheric Research Program (GARP) and the First GARP Global Experiment (FGGE) was adapted. This format had the added advantage of easier access to the FGGE data.

Although the theory underlying the MVOI can be found in numerous papers, it is given in complete form in sections 2 through 5. Much of the basic work was patterned after Lorenc et al. (1977) and Lorenc (1981). The additional work of Daley (1985) to include parameters for geostrophic coupling and for relative magnitudes of the divergence and rotational components of wind are also included.

Covariance computations on polar coordinates and transformation to a Cartesian grid greatly simplify computations; these also are presented in complete form.

Code validation is an extremely important part of any system development. From the extensive literature describing MVOI methods, ways of testing these characteristics can be found. The methods most valuable in locating design and coding errors are presented in section 6. These methods made the implementation of the analysis methods relatively error free, although it is believed that totally error-free code may not be possible (Parnas, 1985; Meyers, 1986).

The methods used to select the data can make a difference in the smoothness and accuracy of the analysis (Barker, 1991). The data selection procedure picks observations for volumes of grid points, and the size of the volumes is determined by observation density. The strategy used for this data selection procedure is given in section 7.

Vector computers, such as the CYBER 205, are most efficient when the software is designed so that computations are done on strings of contiguous variables. The computer is then able to compute values in an assembly line fashion, resulting in ten-fold increases in computation rates. The contiguous strings, or vectors, require special planning starting with the theoretical foundation. For example, use of the volume method of Lorenc (1981), where data values are selected and the analysis is made for volumes of grid points vice individual grid points, make it possible to compose computational strings of over 300 data values. The computational vector length, therefore, is typically in excess of 300 operations long.

Even though MVOI theory was introduced into the meteorological literature over 30 years ago, the MVOI techniques have undergone dramatic improvement over the last 10 years. Much of this improvement is due to the increased power of computers. However, to achieve the added performance, the design of MVOI requires special consideration for setting up the computation for vector and multiprocessor computers.

Finally, some recommendations are presented in section 8 that serve to point out some of the weaknesses discovered in the system, and to make some recommendations for further research.

2.0 Horizontal Covariances

The underlying theory of optimum interpolation requires an accurate description of prediction and observation errors to produce a truly optimal solution. Unfortunately, optimal theory becomes too complicated except

when the error structure of the predication model is assumed stationary and homogeneous. This has lead some investigators to class MVOI as commonly used as a statistical method rather than an optimal one (McPherson et al., 1979) since the true optimal solution would be lost with such simplifying assumptions. Nevertheless, it is hoped that the models used to represent the prediction errors produce all but the minor improvements that would be gained from precise statistical models.

When a simple covariance model is assumed, the short-term prediction error correlations become:

$$\langle \psi_i \psi_j \rangle = \langle \psi^2 \rangle F(r_{ij}) \quad (1)$$

$$\langle \chi_i \chi_j \rangle = \langle \chi^2 \rangle G(r_{ij}), \quad (2)$$

and

$$\langle \phi_i \phi_j \rangle = \langle \phi^2 \rangle E(r_{ij}), \quad (3)$$

where ψ is streamfunction, χ is velocity potential, and ϕ is geopotential; r_{ij} is the distance between two arbitrary points i and j ; F , G , and E are the covariance models for ψ , χ , and ϕ , respectively; the angle brackets symbolize an ensemble average operator; and $\langle \psi^2 \rangle$, $\langle \chi^2 \rangle$, and $\langle \phi^2 \rangle$ are the prediction error variances.

The covariance of the predicted estimate errors between ψ and χ is defined as

$$\langle \psi_i \chi_j \rangle = \langle \chi_i \psi_j \rangle = \sqrt{\langle \psi^2 \rangle \langle \chi^2 \rangle} H(r_{ij}), \quad (4)$$

where H is the covariance model.

Using the Cartesian definition for distance

$$r_{ij} = \sqrt{(x_i - x_j)^2 + (y_i - y_j)^2}, \quad (5)$$

the partial derivatives in Cartesian space operating on an arbitrary function $A(r_{ij})$ becomes

$$\frac{\partial A}{\partial x_i} = A' \frac{\partial r}{\partial x_i} = A' \frac{(x_i - x_j)}{\sqrt{(x_i - x_j)^2 + (y_i - y_j)^2}} = \frac{x_i - x_j}{r} A', \quad (6)$$

$$\frac{\partial A}{\partial x_j} = \frac{x_j - x_i}{r} A', \quad (7)$$

and

$$\frac{\partial A}{\partial y_j} = \frac{y_j - y_i}{r} A' . \quad (8)$$

In these equations and those that follow, the subscripts on r are dropped because they are not necessary for clarity.

Second, partial derivatives in Cartesian coordinate space operating on A have the following form:

$$\frac{\partial^2 A}{\partial y_i \partial x_j} = \frac{\partial}{\partial y_i} \left(\frac{x_j - x_i}{r} A' \right) = - \frac{(y_i - y_j)(x_i - x_j)}{r^2} \left[A'' - \frac{A'}{r} \right] , \quad (9)$$

$$\frac{\partial^2 A}{\partial x_i \partial y_j} = - \frac{(x_i - x_j)(y_i - y_j)}{r^2} \left[A'' - \frac{A'}{r} \right] , \quad (10)$$

$$\frac{\partial^2 A}{\partial x_i \partial x_j} = - \frac{A'}{r} - \frac{(x_i - x_j)^2}{r^2} \left[A'' - \frac{A'}{r} \right] , \text{ and} \quad (11)$$

$$\frac{\partial^2 A}{\partial y_i \partial y_j} = - \frac{A'}{r} - \frac{(y_i - y_j)^2}{r^2} \left[A'' - \frac{A'}{r} \right] . \quad (12)$$

With the relations above, the covariances defined by equations (1) and (2) can be converted to measurable quantities, u , the wind along the x -axis, and v , the wind along the y -axis. Substituting the relationships between streamfunction, velocity potential, and wind,

$$u = - \frac{\partial \psi}{\partial y} + \frac{\partial \chi}{\partial x} , \quad (13)$$

and

$$v = - \frac{\partial \psi}{\partial x} + \frac{\partial \chi}{\partial y} . \quad (14)$$

The equation for spatial covariances for the u -component of wind becomes:

$$\begin{aligned} \langle u_i u_j \rangle &= \left\langle \left(- \frac{\partial \psi_i}{\partial y_i} + \frac{\partial \chi_i}{\partial x_i} \right) \left(- \frac{\partial \psi_j}{\partial y_j} + \frac{\partial \chi_j}{\partial x_j} \right) \right\rangle \\ &= \left\langle \frac{\partial \psi_i}{\partial y_i} \frac{\partial \psi_j}{\partial y_j} \right\rangle - \left\langle \frac{\partial \chi_i}{\partial x_i} \frac{\partial \psi_j}{\partial y_j} \right\rangle - \left\langle \frac{\partial \psi_i}{\partial y_i} \frac{\partial \chi_j}{\partial x_j} \right\rangle + \left\langle \frac{\partial \chi_i}{\partial x_i} \frac{\partial \chi_j}{\partial x_j} \right\rangle . \end{aligned} \quad (15)$$

It is reasonable and much simpler to assume that the rotational component of the atmospheric motion is uncorrelated with the divergent component so that $\langle \chi_i \psi_j \rangle = \langle \chi_j \psi_i \rangle = 0$, and

$$\begin{aligned} \langle u_i u_j \rangle &= \frac{\partial^2}{\partial y_i \partial y_j} \langle \psi_i \psi_j \rangle + \frac{\partial^2}{\partial x_i \partial x_j} \langle \chi_i \chi_j \rangle \\ &= -\frac{1}{r} \frac{d \langle \psi_i \psi_j \rangle}{dr} - \frac{(y_i - y_j)^2}{r^2} [\Re(\langle \psi_i \psi_j \rangle)] \\ &\quad - \frac{1}{r} \frac{d \langle \chi_i \chi_j \rangle}{dr} - \frac{(x_i - x_j)^2}{r^2} [\Re(\langle \chi_i \chi_j \rangle)] . \end{aligned} \quad (16)$$

where \Re is a derivative operator with respect to r defined as

$$\Re(A) = A'' - \frac{A'}{r} . \quad (17)$$

The $v_i - v_j$ covariances are similarly derived so that

$$\begin{aligned} \langle v_i v_j \rangle &= -\frac{1}{r} \frac{d \langle \psi_i \psi_j \rangle}{dr} - \frac{(x_i - x_j)^2}{r^2} [\Re(\langle \psi_i \psi_j \rangle)] \\ &\quad - \frac{1}{r} \frac{d \langle \chi_i \chi_j \rangle}{dr} - \frac{(y_i - y_j)^2}{r^2} [\Re(\langle \chi_i \chi_j \rangle)] . \end{aligned} \quad (18)$$

Finally, for the $u_i - v_j$ covariances

$$\begin{aligned} \langle u_i v_j \rangle &= \langle v_i u_j \rangle = + \frac{(x_i - x_j)(y_i - y_j)}{r^2} [\Re(\langle \psi_i \psi_j \rangle)] \\ &\quad - \frac{(x_i - x_j)(y_i - y_j)}{r^2} [\Re(\langle \chi_i \chi_j \rangle)] . \end{aligned} \quad (19)$$

The covariances (16), (18), and (19) are simplified by transforming winds to cylindrical coordinates, which is a coordinate system in the radial direction, r , and the angle this direction makes with the x -axis, θ , i.e.,

$$\mathbf{v}' = \mathbf{c} \mathbf{v} \quad (20)$$

where

$$\mathbf{v} = \begin{pmatrix} u \\ v \end{pmatrix} . \quad (21)$$

$$\mathbf{v}' = \begin{pmatrix} u' \\ v' \end{pmatrix}, \quad (22)$$

and

$$\mathbf{c} = \begin{pmatrix} \cos \theta & \sin \theta \\ -\sin \theta & \cos \theta \end{pmatrix}. \quad (23)$$

The values u' and v' are the normal and tangential velocity components respectively.

Since

$$\mathbf{c}^{-1} = \text{Adjoint } \mathbf{c}, \quad (24)$$

the reverse of equation (20) is simply

$$\mathbf{v} = \text{Adjoint } \mathbf{c} \mathbf{v}'. \quad (25)$$

Using

$$\frac{x_j - x_i}{r} = \cos \theta \quad (26)$$

and

$$\frac{y_j - y_i}{r} = \sin \theta, \quad (27)$$

to solve for the velocity covariances in cylindrical coordinates yields:

$$\begin{aligned} \langle u'_i u'_j \rangle &= \langle (u_i \cos \theta + v_i \sin \theta) (u_j \cos \theta + v_j \sin \theta) \rangle \\ &= \langle u_i u_j \rangle \cos^2 \theta + 2 \langle u_i v_j \rangle \sin \theta \cos \theta + \langle v_i v_j \rangle \sin^2 \theta, \end{aligned} \quad (28)$$

or

$$\langle u'_i u'_j \rangle = -\frac{1}{r} \frac{d \langle \psi_i \psi_j \rangle}{dr} - \frac{d^2 \langle \chi_i \chi_j \rangle}{dr^2}. \quad (29)$$

Similarly,

$$\langle v'_i v'_j \rangle = -\frac{d^2 \langle \psi_i \psi_j \rangle}{dr^2} - \frac{1}{r} \frac{d \langle \chi_i \chi_j \rangle}{dr}, \quad (30)$$

and

$$\langle u'_i v'_j \rangle = \langle v'_i u'_j \rangle = 0. \quad (31)$$

These covariances are now easily computed once the relations (1) and (2) are defined.

To obtain the covariances between geopotential, ϕ , and wind, the covariances are first defined in Cartesian coordinates where

$$\begin{aligned}\langle \phi_i u_j \rangle &= \left\langle \left(\phi_i \right) \left(-\frac{\partial \psi_j}{\partial y_j} + \frac{\partial \chi_j}{\partial x_j} \right) \right\rangle \\ &= -\frac{y_j - y_i}{r} \frac{d \langle \phi_i \psi_j \rangle}{dr} + \frac{x_j - x_i}{r} \frac{d \langle \phi_i \chi_j \rangle}{dr},\end{aligned}\quad (32)$$

$$\langle u_i \phi_j \rangle = -\langle \phi_i u_j \rangle, \quad (33)$$

$$\begin{aligned}\langle \phi_i v_j \rangle &= \left\langle \left(\phi_i \right) \left(-\frac{\partial \psi_j}{\partial x_j} + \frac{\partial \chi_j}{\partial y_j} \right) \right\rangle \\ &= -\frac{x_j - x_i}{r} \frac{d \langle \phi_i \psi_j \rangle}{dr} + \frac{y_j - y_i}{r} \frac{d \langle \phi_i \chi_j \rangle}{dr},\end{aligned}\quad (34)$$

and

$$\langle v_i \phi_j \rangle = -\langle \phi_i v_j \rangle. \quad (35)$$

Covariances for a geostrophically coupled system can be modeled using

$$\langle \phi_i \psi_j \rangle = \langle \psi_i \phi_j \rangle = \frac{\mu}{f} \langle \phi_i \phi_j \rangle \sqrt{\frac{F(r)}{E(r)}}, \quad (36)$$

and

$$\langle \phi_i \chi_j \rangle = \langle \chi_i \phi_j \rangle = 0, \quad (37)$$

where f is the Coriolis parameter and μ is a function of the degree of geostrophic coupling desired in the final analysis. As μ ranges from 0 to 1, the modeled covariance between wind and geopotential ranges from 0, uncoupled, to 1, full geostrophic coupling. Fractional values of μ result in a partially geostrophic system as discussed in Daley (1985). Substituting equation (36) into equation (32) and equation (34) gives

$$\langle \phi_i u_j \rangle = -\frac{y_j - y_i}{r} \frac{\mu}{f} \frac{d \langle \phi_i \phi_j \rangle}{dr} \sqrt{\frac{F(r)}{E(r)}}, \quad (38)$$

and

$$\langle \phi_i v_j \rangle = \frac{x_j - x_i}{r} \frac{\mu}{f} \frac{d \langle \phi_i \phi_j \rangle}{dr} \sqrt{\frac{F(r)}{E(r)}}. \quad (39)$$

Assuming the autocovariance function for ψ , $F(r)$, is the same as that for ϕ , $E(r)$, and using equations (26), (27), (32), and (34) to derive the covariances in cylindrical coordinates yields:

$$\begin{aligned}\langle \phi_i u_j \rangle &= \langle \phi_i u_j \rangle \cos \theta + \langle \phi_i v_j \rangle \sin \theta \\ &= 0 ,\end{aligned}\tag{40}$$

and

$$\begin{aligned}\langle \phi_i v_j \rangle &= \langle \phi_i v_j \rangle \sin \theta + \langle \phi_i u_j \rangle \cos \theta \\ &= \frac{\mu}{f} \frac{d \langle \phi_i \phi_j \rangle}{dr} \sqrt{\frac{F(r)}{E(r)}} .\end{aligned}\tag{41}$$

It is possible to model the amount of divergence or rotation in the predicted estimate wind error through an appropriate choice of covariance model for χ and ψ . Since $E(r_{ij})$ is readily determined from observations, it is convenient to define

$$F(r) = (1-v)E(r) ,\tag{42}$$

and

$$G(r) = vE(r) .\tag{43}$$

The variable v then becomes the parameter to model the divergence that exists in the wind field. As v approaches 1, the wind error models become fully divergent, and as v approaches 0, the wind models become rotational.

The covariance models (3), (29), (30), and (41) have now been formulated so that:

- There are two parameters to control the constraints in the analysis: μ , which controls the geostrophic coupling, and v , which controls the divergence.
- They are in cylindrical coordinates, which is simpler than in Cartesian coordinates, and $\langle u_i' v_j' \rangle$, $\langle v_i' u_j' \rangle$, $\langle v_i' \phi_j' \rangle$, and $\langle \phi_i' v_j' \rangle$ do not have to be computed since they are zero.
- Their computation is independent of the projection of the analysis grid.
- They only depend on the function chosen for the normalized covariance model for geopotential, $E(r_{ij})$.

The treatment of error functions in this section assumed that the vertical structure was independent of the horizontal structure. This makes the computations much faster than using a fully three-dimensional structure function, and the mathematics are also easier. The vertical structure formulations are presented in the next section.

3.0 Vertical Covariances

The definition of the vertical geopotential covariance is defined as

$$\langle \phi_i \phi_k \rangle = \sqrt{\langle \phi_i^2 \rangle} \sqrt{\langle \phi_k^2 \rangle} H(p_i, p_k), \quad (44)$$

where the subscripts refer to two arbitrary pressure levels p_i and p_k , and H is the normalized vertical covariance function for geopotential and a function of the pressure levels.

The geostrophic coupling relations are complicated for vertical covariances unless the normalized vertical covariance is the same for both wind and geopotential. Consequently, the wind vertical covariances take the form of equation (44) except ϕ is replaced by u or v .

Satellites do not provide a reference such as surface pressure to their soundings, so the temperature they measure can only be converted to geopotential thickness, unless a reference level is separately analyzed beforehand. Lorenc (1981) established the covariances for thickness so that the satellite temperatures could be used directly. This makes the use of thickness information more mathematically precise, as the optimality does not have to account for the errors in a separately derived reference level.

The vertical thickness covariance is

$$\begin{aligned} \langle D_i D_k \rangle &= \langle (\phi_i - \phi_{i-1})(\phi_k - \phi_{k-1}) \rangle \\ &= \langle \phi_i \phi_k \rangle - \langle \phi_{i-1} \phi_k \rangle - \langle \phi_i \phi_{k-1} \rangle + \langle \phi_{i-1} \phi_{k-1} \rangle, \end{aligned} \quad (45)$$

where the individual terms are evaluated from equation (44).

Thickness correlated with any other variable such as A_k is

$$\langle D_i A_k \rangle = \langle \phi_i A_k \rangle - \langle \phi_{i-1} A_k \rangle. \quad (46)$$

4.0 Variable Scaling

The optimum interpolation equations are typically simplified by normalizing the variables by the prediction error variance. These normalization constants can be tricky, and if done incorrectly, they destroy the geostrophic and rotational flow constraints, as well as the statistical properties of the optimization.

The velocity covariance relations, equations (29) and (30), evaluated in the limit as point separation goes to zero, form the basis for the scaling values, i.e.,

$$\langle u^2 \rangle = \lim_{r \rightarrow 0} \left[-\frac{1}{r} \frac{d \langle \psi_i \psi_j \rangle}{dr} - \frac{d^2 \langle \chi_i \chi_j \rangle}{dr^2} \right] \quad (47)$$

and

$$\langle v^2 \rangle = \lim_{r \rightarrow 0} \left[-\frac{d^2 \langle \psi_i \psi_j \rangle}{dr^2} - \frac{1}{r} \frac{d \langle \chi_i \chi_j \rangle}{dr} \right]. \quad (48)$$

The prediction error estimate of the wind is computed from the background or first-guess wind error variance because its dependence on latitude is much smaller than the geopotential first-guess error variance. Then the geopotential first-guess error variance is estimated from the error covariance relationships. To make the scaling values compatible with geostrophic coupling, the geostrophic coupling parameter, μ , is set to 1 for full coupling and the divergence parameter, ν , is set to 0 for nondivergent flow. The streamfunction prediction error variance is estimated from the geostrophic approximation, $\frac{\phi_p}{f}$, where ϕ_p^2 is the error variance of the predicted estimate of geopotential, and as such becomes the square of the scaling factor for geopotential. The relationship for the scaling constants is

$$\langle v_p^2 \rangle = \left(\frac{\phi_p}{f} \right)^2 \lim_{r \rightarrow 0} \left(\frac{d^2 E(r)}{dr^2} \right) \quad (49)$$

and

$$\langle u_p^2 \rangle = \left(\frac{\phi_p}{f} \right)^2 \lim_{r \rightarrow 0} \left(\frac{1}{r} \frac{dE(r)}{dr} \right), \quad (50)$$

where the subscript p designates the prediction error variance.

The relationship

$$\lim_{r \rightarrow 0} \frac{d^2 E(r)}{dr^2} = \lim_{r \rightarrow 0} \frac{1}{r} \frac{dE(r)}{dr}, \quad (51)$$

and the condition that the normalized model for geopotential, E , be twice differentiable in the limit as r goes to zero (see Franke, et al., 1988) makes possible the definition

$$c_v^2 = \lim_{r \rightarrow 0} \left(-\frac{1}{r} \frac{dE(r)}{dr} \right). \quad (52)$$

The wind and geopotential scaling values are therefore related by

$$u_p^2 = v_p^2 = \left(\frac{\phi_p}{f} \right)^2 c_v^2. \quad (53)$$

This relation must be satisfied if the geostrophic and rotational flow constraints are to be imposed.

Wind variance is nearly the same in the tropics as it is in the mid-latitudes, whereas geopotential variance decreases from midlatitudes to the tropics. As a result, the scaling variances are determined by verifying short-term predictions of wind against observations, and then computing geopotential scaling constants from equation (53).

Thickness scaling is computed from equation (45), where

$$\begin{aligned} \left[D_p^2(p_k) \right]^2 &= \phi_p^2(p_k) H(p_k, p_k) \\ &\quad - 2\phi_p(p_k) \phi_p(p_{k-1}) H(p_k, p_{k-1}) \\ &\quad + \phi_p^2(p_{k-1}) H(p_{k-1}, p_{k-1}). \end{aligned} \quad (54)$$

5.0 Optimizing the Analysis

Meteorological analysis methods typically involve the computation of a weighted average of observation values. Written in general vector matrix form, the analysis at a specific point, k , is

$$r_k = w_k^T \begin{bmatrix} b_1 - p_1 \\ \vdots \\ b_i - p_i \end{bmatrix}, \quad (55)$$

where $b_i - p_i$ is the difference between the observation value and the prediction value, r_k is the analyzed increment, and w is the column matrix containing the weighting coefficients. Optimization of this equation can be done in many ways and with different levels of success, depending on the assumptions necessary to keep the solution tractable. The optimum interpolation analysis method that evolved through the works of Gandin (1963), Rutherford (1976, 1978), Schlatter (1975), Bergman (1976, 1979), Lorenc (1981), Daley (1985), and others is the basis for the optimization method adapted for this analysis. This analysis method requires that the mean-squared error of the analysis be minimized over statistically significant realizations. The limitations of this optimization are caused by the assumption of stationarity and homogeneity in the computation of the variable covariances and in the inexact determination of the statistical parameters used.

This description closely follows the one presented by Lorenc (1981) and Daley (1985, 1991), except that more steps are provided in the derivations to make them easier to follow.

Minimization of analysis error requires the definition of the following error parameters:

- Analysis error is $a = A - T$, where A is the analyzed value and T is the true value.
- Observation error is $b = B - T$, where B is the observed value.
- Prediction error is $p = P - T$, where P is the predicted value.
- Analysis error estimate is $E^a = \langle a^2 \rangle^{1/2}$.
- Observation error estimate is $E^o = \langle b^2 \rangle^{1/2}$.
- Prediction error estimate is $E^p = \langle p^2 \rangle^{1/2}$.
- The error parameters scaled by the prediction error estimate are:

$$\epsilon^o = \frac{E^o}{E^p}, \quad (56)$$

$$\epsilon^a = \frac{E^a}{E^p}, \quad (57)$$

$$q = \frac{B-P}{E^p}, \quad (58)$$

$$r = \frac{A-P}{E^p}, \quad (59)$$

$$\pi = \frac{P}{E^p}, \quad (60)$$

$$\alpha = \frac{a}{E^a}, \quad (61)$$

$$\beta = \frac{b^o}{E^o}, \text{ and} \quad (62)$$

$$\epsilon^o \alpha = \frac{a}{E^a} \frac{E^o}{E^p}. \quad (63)$$

The analysis equation scaled by the values of expected error is

$$\left(\frac{a}{E^p} - \frac{p}{E^p} \right)_k = \mathbf{w}_k^T \begin{bmatrix} \frac{b_1}{E^o} \frac{E^o}{E^p} - \frac{p_1}{E^p} \\ \vdots \\ \frac{b_i}{E^o} \frac{E^o}{E^p} - \frac{p_i}{E^p} \end{bmatrix}, \quad (64)$$

which leads to the equation for analysis error

$$\alpha_k \epsilon_k^a = \pi_k + \mathbf{w}_k^T \begin{bmatrix} \beta_1 \epsilon^o - \pi_1 \\ \vdots \\ \beta_i \epsilon^o - \pi_i \end{bmatrix}. \quad (65)$$

Squaring the analysis error equation (65); taking the ensemble average; then using the following relations:

$$\langle \alpha_k^2 \rangle = \left\langle \frac{a_k}{E^a} \right\rangle^2 = \left(\frac{E^a}{E^a} \right)^2 = 1 \quad (66)$$

$$\langle \pi_k^2 \rangle = \frac{\langle p_k^2 \rangle}{(E^p)^2} = 1; \quad (67)$$

gives the squared analysis error equation,

$$\left(\epsilon_k^a\right) = 1 - 2 \mathbf{w}_k^T \mathbf{h}_k + \mathbf{w}_k^T \mathbf{M} \mathbf{w}_k, \quad (68)$$

where

$$\mathbf{M} = \begin{bmatrix} m_{11} & \cdots & m_{1n} \\ \cdots & m_{ij} & \cdots \\ m_{n1} & \cdots & m_{nn} \end{bmatrix}, \quad (69)$$

$$m_{ij} = \langle \pi_i \pi_j \rangle - \epsilon_i^o \langle \beta_i \beta_j \rangle \epsilon_j^o - \epsilon_i^o \langle \beta_i \pi_j \rangle - \langle \pi_i \beta_j \rangle \epsilon_j^o, \quad (70)$$

and

$$\mathbf{h} = \begin{bmatrix} \langle \pi_k \pi_1 \rangle - \langle \pi_k \beta_1 \rangle \epsilon_1^o \\ \vdots \\ \langle \pi_k \pi_i \rangle - \langle \pi_k \beta_i \rangle \epsilon_i^o \end{bmatrix}. \quad (71)$$

The optimality in the analysis occurs when the differentiation of (68) with respect to the weighting coefficients, \mathbf{w}_k , is set to zero, which leads to

$$\mathbf{w}_k = \mathbf{M}^{-1} \mathbf{h}_k. \quad (72)$$

The analysis equation, (55), in optimal form is therefore

$$\mathbf{r}_k = \mathbf{h}_k^T \mathbf{M}^{-1} \mathbf{q}. \quad (73)$$

The last two terms of this equation are independent of the analysis grid location, k , so they can be combined into a single term

$$\mathbf{c} = \mathbf{M}^{-1} \mathbf{q}. \quad (74)$$

This simplifies the analysis computation to

$$\mathbf{r}_k = \mathbf{c}^T \mathbf{h}_k. \quad (75)$$

The term (74) only needs computing each time the observations being used are changed. Observation selections that span relatively large volumes can be used for numerous gridpoints, reducing computation to a simple inner product of two column vectors for all but the first grid point. This simplification makes the volume method, where observation selections are made for volumes of gridpoints rather than individual ones, cost effective. This is especially true where observations are sparse. On a spherical grid the converging meridians near the poles create densely spaced gridpoints, so that about 20% of the total gridpoints are easily assigned to the two polar volumes.

Substitution of equation (72) into equation (68) gives the equation for the expected analysis error

$$(\epsilon_k^a)^2 = 1 - \mathbf{h}_k^T \mathbf{M}^{-1} \mathbf{h}_k. \quad (76)$$

The expected analysis errors are useful in the comparison of strategies for observation utilization, but are not needed during the operational analysis.

Even though much effort goes into removing observations contaminated for one reason or another (see Baker, 191 a-d), some remain questionable and require further checking by the internal quality control procedures. The steps to the internal quality control are the following:

1. Questionable observations are tagged. An observation becomes questionable when it either marginally passes the external quality control, or it departs from the background fields by an amount that exceeds three times the expected error variance.
2. Observations that depart from the background field by an amount that exceeds five times the expected error are tagged for gross rejection.
3. The change in the analysis done to a questionable observation is evaluated by comparing the analysis at the location of the observation with and without the observation.
4. If the change due to the observation exceeds expected tolerances, then it is rejected by the analysis.
5. Rejected observations are kept in the analysis, but their weight is constrained to zero. This is done without resolving equation (74).

The mathematics used to determine the change done to an individual observation, its expected change, and procedures for constraining the weights of rejected observations to zero are presented below. These equations are also found in Rutherford (1978) and Lorenc (1981) in more abbreviated form. The expected change of an individual observation is related to the variance between the analysis and that observation,

$$\langle r_k - q_k \rangle^2 = \langle r_k^2 \rangle - 2 \langle r_k q_k \rangle + \langle q_k^2 \rangle. \quad (77)$$

Substituting equation (55) gives

$$r_k^2 = \mathbf{w}_k^T \langle \mathbf{q}_k \mathbf{q}_k^T \rangle \mathbf{w}_k. \quad (78)$$

Since

$$\mathbf{q} = \begin{bmatrix} \epsilon_1^o \beta_1 - \pi_1 \\ \vdots \\ \epsilon_i^o \beta_i - \pi_i \end{bmatrix}, \quad (79)$$

it follows that

$$\langle \mathbf{q}\mathbf{q}^T \rangle = \mathbf{M}, \quad (80)$$

and

$$\langle r_k q_k \rangle = \mathbf{w}_k^T \langle \mathbf{q}\mathbf{q} \rangle = \mathbf{w}_k^T \mathbf{m}_k, \quad (81)$$

where \mathbf{m}_k is the k^{th} column of \mathbf{M} .

The average squared difference between analysis and observation is now

$$\langle r_k - q_k \rangle^2 = \mathbf{w}_k^T \mathbf{M} \mathbf{w}_k - 2 \mathbf{w}_k^T \mathbf{m}_k + 1 + (\epsilon_k^o)^2. \quad (82)$$

Minimizing this equation through optimization of the weight coefficients gives

$$\mathbf{M} \mathbf{w}_k + \mathbf{w}_k^T \mathbf{M} - 2 \mathbf{m}_k = 0, \quad (83)$$

or

$$\mathbf{w}_k^T = \mathbf{M}^{-1} \mathbf{m}_k = \mathbf{d}_k. \quad (84)$$

The vector \mathbf{d}_k is zero except for the k^{th} element, which is one. The minimization of equation (82) with the suspect observation contributing to the analysis is not useful and produces only a trivial solution, and therefore the minimization must be constrained.

Minimizing the averaged squared difference between the analysis and observation subject to the constraint that selected observations are given zero weight requires that equation (82) be minimized subject to the constraints

$$\mathbf{d}_m^T \mathbf{w}_k = 0 \quad \forall m \in l, \quad (85)$$

where $\forall m \in l$ is to be read for all m from the set that makes up the list of rejected observations, l .

A constrained minimization of the analysis error can be achieved with variational calculus, or

$$\langle r_k - q_k \rangle^2 = \mathbf{w}_k^T \mathbf{M} \mathbf{w}_k - 2 \mathbf{w}_k^T \mathbf{m}_k + 1 + (\epsilon_k^o)^2 - 2 \sum_{\substack{m \\ \forall m}}^{\epsilon l} \lambda_m^k \mathbf{d}_m^T \mathbf{w}_k, \quad (86)$$

where λ_m^k is the Lagrange multiplier used to insure the constraint, equation (85), is exactly satisfied. Taking the first variation of equation (86) with respect to \mathbf{w}_k and λ_m^k , and setting the result to zero, gives an equation set whose solution is the optimum column matrix, \mathbf{w}_k , that gives zero weighting to the rejected observations, i.e.,

$$0 = 2\mathbf{w}_k \mathbf{M} - 2\mathbf{m}_k + 2\mathbf{D} \lambda_k + 2\mathbf{D}^T \mathbf{w}_k, \quad (87)$$

The columns of \mathbf{D} are made of $\mathbf{d}_m \forall m \in l$. To solve for λ_k , \mathbf{w}_k is eliminated by multiplying both sides of this equation by \mathbf{M}^{-1} and then \mathbf{D}^T , or

$$\lambda_k = -[\mathbf{D}^T \mathbf{M}^{-1} \mathbf{D}]^{-1} \mathbf{D}^T \mathbf{d}_k. \quad (88)$$

The expected change caused by an individual observation is computed by substitution of equations (85) and (72) into equation (86), or

$$\langle r_k - q_k \rangle^2 = \left(\epsilon_k^0 \right)^2 + 1 - \mathbf{w}_k^T \mathbf{m}_k. \quad (89)$$

Observations are rejected when they cause a change that exceeds their expected change according to

$$\langle r_k - q_k \rangle^2 > T^2 [\langle r_k - q_k \rangle^2 + 0.1]. \quad (90)$$

The value of the tolerance, T , is used to tune the rejection, and the analysis, r_k , excludes the observation at k and others already rejected. This method of evaluation is a way to compare an individual observation with all of the other observations and the first guess. It even accounts for differences in observation density, where an individual observation is expected to impact an analysis more over data sparse than data-dense areas.

Each questionable observation is tested using equation (90). Once all the observations that fail the test are identified, the solution for optimal weights is again computed through minimization of the equation for the ensemble average of squared analysis error, but this time subject to the constraint that the rejected observations have zero weight. The optimum solution comes from minimization of

$$\left(\epsilon_k^a \right)^2 = 1 - 2\mathbf{w}_k^T \mathbf{h}_k + \mathbf{w}_k^T \mathbf{M} \mathbf{w}_k \sum_{\forall m}^{\epsilon l} \lambda_m^k \mathbf{d}_m^T \mathbf{w}_k, \quad (91)$$

with respect to the independent variables \mathbf{w}_k and λ_m^k . This gives

$$0 = -2\mathbf{h}_k + 2\mathbf{w}_k^T \mathbf{M} + 2\mathbf{D} \lambda_k + 2\mathbf{D}^T \mathbf{w}_k. \quad (92)$$

Multiplying both sides of this equation by \mathbf{M}^{-1} and \mathbf{D} eliminates \mathbf{w}_k , thereby giving the solution for the Lagrange multiplier,

$$\lambda_k = -(\mathbf{D}^T \mathbf{M}^{-1} \mathbf{D})^{-1} \mathbf{D}^T \mathbf{M}^{-1} \mathbf{h}_k. \quad (93)$$

Substituting this equation into the equation for weighting coefficients, equation (92), gives the final equation for the optimum weighting coefficients,

$$\mathbf{w}_k = \mathbf{M}^{-1}\mathbf{h}_k - \mathbf{M}^{-1}\mathbf{D}(\mathbf{D}^T \mathbf{M}^{-1}\mathbf{D})^{-1}\mathbf{D}^T \mathbf{M}^{-1}\mathbf{h}_k. \quad (94)$$

The final analysis with rejected observations removed becomes

$$\mathbf{r}_k = \mathbf{h}_k^T (\mathbf{M}^{-1} - \mathbf{M}^{-1}\mathbf{D}[\mathbf{D}^T \mathbf{M}^{-1}\mathbf{D}]^{-1}\mathbf{D}^T \mathbf{M}^{-1})\mathbf{q}. \quad (95)$$

Collecting the terms that are independent of the grid point location into a single term gives

$$\mathbf{r}_k = \mathbf{c}_q^T \mathbf{h}_k, \quad (96)$$

where

$$\mathbf{c}_q = [\mathbf{M}^{-1} - \mathbf{M}^{-1}\mathbf{D}[\mathbf{D}^T \mathbf{M}^{-1}\mathbf{D}]^{-1}\mathbf{D}^T \mathbf{M}^{-1}]\mathbf{q}. \quad (97)$$

This equation represents the optimum analysis subject to the constraint that rejected observations have zero weight. A comparison of the coefficient equation for the optimum solution, (74), with the equation for optimum solution using constraints, (97), reveals that the two solutions can be computed as simply as one, because the second solution is a function of the first. The only additional work required for the second solution is the inversion of $[\mathbf{D}^T \mathbf{M} \mathbf{D}]$, which is a square matrix with order equal to the number of rejected observations. Typically, the solution for 300 observation values will require the inversion of a sixth order matrix, corresponding to 6 rejected values.

The theory above is used in the analysis of observations using the following steps:

1. All observation values are converted to differences between observed and predicted values. This is done by interpolating the gridded prediction to observation location, and subtracting the predicted value from the observed value. The interpolation is done using a cubic-spline algorithm designed to take advantage of the vector speeds on the computer.
2. A grid volume is defined and the observations appropriate for this volume are selected, up to a limit of 300 values.
3. The normalization coefficients are used to convert the observations into nondimensional space.
4. The prediction error covariance models are used to compute the covariances between the observations, and the results are stored in \mathbf{M} .
5. The covariance matrix, \mathbf{M} , is decomposed using Cholesky decomposition. Again, this is done using an algorithm designed to take advantage of the vector speed of the computer. This makes it possible to apply the factor \mathbf{M}^{-1} by multiplication of the matrices that result from the decomposition.
6. The changes in the analysis due to each questionable observation are compared to their expected change using equation (86), and those failing to meet the conditions of equation (90) are rejected.
7. The column matrix (equation 74) is defined from \mathbf{M}^{-1} and the list of rejected observations.

8. For each gridpoint, k , the covariances are computed between observation locations and gridpoint location, and stored in h_k .

9. The inner product between c_k and h_k is computed as in equation (96) to get the analysis at location k .

10. The previous two steps are repeated through all points on the grid.

11. The normalization coefficients are used to convert the analysis to dimensional space.

12. Steps 2 through 11 are repeated until all grid volumes are complete, then the grid volumes are meshed with each other to form the completed analysis increment.

13. The increments are interpolated to the model coordinates and added to the prediction values. This updates the prediction model, thereby generating the analysis.

The bulk of the computer code used to generate an analysis from the steps above is in the data base interfaces, the observation sorting, selection, and tagging. It is difficult to validate this code except to track individual data values through the process, which was done in a variety of ways. The theory, likewise, is difficult to validate because of the lack of analytic examples to generate exact cases. Some of the validation tests that illustrate features of the analysis are given in the next section.

6.0 Validation of Analysis System

In the development of prediction models, the accuracy of the numerical product is frequently compared against a known result. The nature of objective analysis methods does not typically require that this be done unless one wishes to insure against coding or design errors whose effect is too small to be detected when the system is exposed to imperfect real situations. This insurance against small errors is valuable because it is these errors that go undetected for years, and cause sophisticated analysis methods to perform as poorly as the less rigorous simple ones.

A complete suite of tests are available to test multivariate optimum interpolation against theory. The ability of the analysis system to retain constraints, the impact of observational correlated error, the accuracy of the vertical interpolation, the impact of the poles in the spherical grid, the computation of the covariance model from analytical fields, and a nonlinear-least-squares fitting algorithm have been tested. These tests are also valuable in their illustration of the strengths of the multivariate optimum interpolation methodology. A few of the more important tests are given here to demonstrate the features built into the program.

6.1 Analysis Constraints

Two constraints can be imposed through the proper selection of the appropriate parameters when the covariances are computed.

The geostrophic constraint is controlled by the parameter μ , which must be set to one for full geostrophic coupling. Since the geostrophic constraint is also nondivergent, the divergence parameter, v , must be set to zero to give a purely rotational wind field.

The geostrophic constraint was tested using a line of gridpoints 10 km apart. Observations were located at the endpoints of this line. The analyzed

winds were then compared with the wind computed from the centered finite difference equivalence of $u = -f \nabla_x \phi$. The results of this experiment are shown in Figure 1 for the right-hand side of the grid, since the solutions are symmetrical about the center. As shown in Figure 1, the computed and analyzed winds were identical to each other, illustrating that the geostrophic constraint is precise. It should be remembered that the analysis constraints are only imposed on the increments between the analysis and the prediction, and not the total field. Applied only to the increments, it can be argued that the nonlinear effects are negligible and that the geostrophic coupling is satisfactory. Williamson and Daley (1983) discovered situations where the nonlinear component is important, and they proposed a unified method to overcome the deficiency. Their method adjusts nonlinear components of the flow through iteration between the analysis and initialization; a technique that should be tested with the Navy system.

Even though the parameters may be set for full coupling between winds and heights, the resulting analysis may lack this coupling. This is caused by two factors:

1. The grid used to compute geostrophic winds may lack the resolution required to pick up the gradients that exist on the analysis surface, and
2. The observations used to analyze one area may not be used to analyze an adjacent area.

This latter factor is illustrated in Figure 2 where the observations used over the center half of the grid were different from the ones used over the outer quarters; the center half of the grid included a wind observation equal to the geostrophic wind computed from the two height observations located at the endpoints. Note the discontinuity in Figure 2 at the boundary between the analysis done with all observations and that done only with heights. The analyzed winds reflect the geostrophic winds of the analysis surface, whereas the computed winds reflect the differences between the two surfaces. This effect may not be obvious where the observations are selected for gridpoints (see

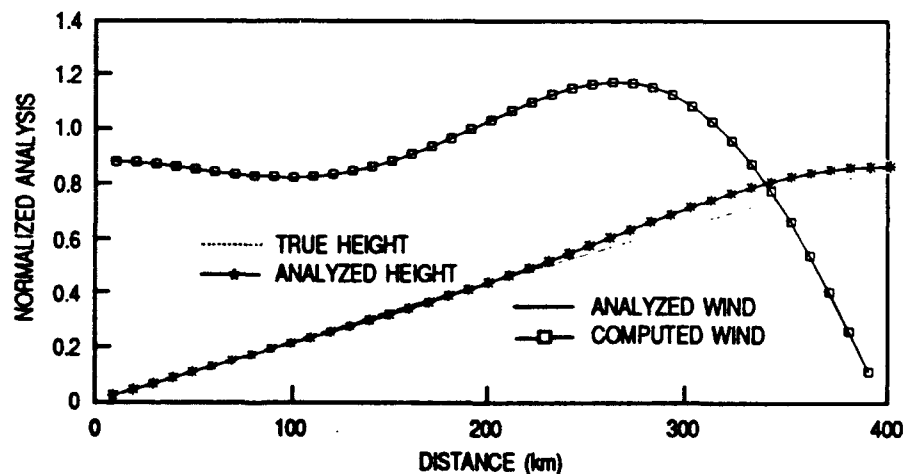


Figure 1. The analyzed pressure height and computed wind from height using the geostrophic relationship plotted with the true solution for height. The analysis was made from two height observations located at +400 km and -400 km, and a single wind observation at the origin.

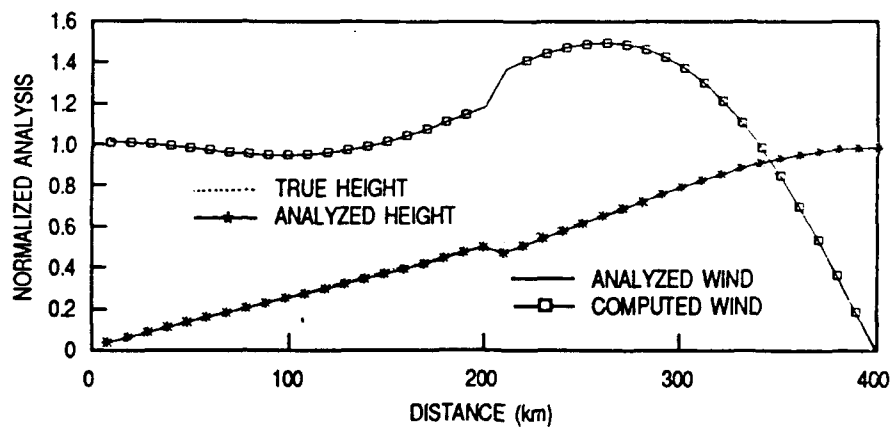


Figure 2. Same as Figure 1 except the left half of the grid was analyzed using a different set of observations from the right side. The discontinuity in the height surface in the center is where the switch from one data set to the other was made.

Barker, 1992), but where they are picked for grid volumes the analysis surface in one volume may be significantly different from the surface in an adjacent volume. Consequently, the volumes are designed so that they overlap and the discontinuity can be made smooth through weighted averaging of the overlapping surfaces. Unfortunately, the constraints are not retained through this averaging procedure.

The constraint governing the divergence is illustrated using a single wind observation at the center of the analysis grid. The results for fully rotational ($v = 0$), fully divergent ($v = 1$), and a mixture of divergent and rotational ($v = .5$) are shown in Figure 3. It is of interest to note that the analysis comprised of both divergent and rotational components produced corrections along the direction of the observed wind only.

The impact of the coupling of a multivariate analysis was tested in a global data assimilation experiment. The system used was NOGAPS version 2 (the current version is 3.2). The fit of the analysis first-guess, which is the predicted values from the previous analysis, was used to measure the success of the two systems. In both experiments, the analysis equally fit the observations, but first-guess errors were about 10% smaller in the coupled system. These results are shown in Figure 4.

6.2 Expected Analysis Error

The expected analysis error is the quantity that is minimized in the optimization of the weighting coefficients used in the analysis. This quantity is useful in the illustration of the power of the optimum interpolation methodology, and it is readily computed from equation (76). The capability of the analysis to effectively utilize various types of observations was illustrated for the following situations: correlated observational error compared to random error; height and wind analysis accuracy compared for computations from height observations alone, wind observations alone, or a combination of heights and winds. These experiments are similar to the ones illustrated by Bengtsson (1976).

Correlated observation error may occur when a single platform, such as a satellite, is used to produce many observations. Should the errors be caused by the instrument or the algorithm that converts the sensor

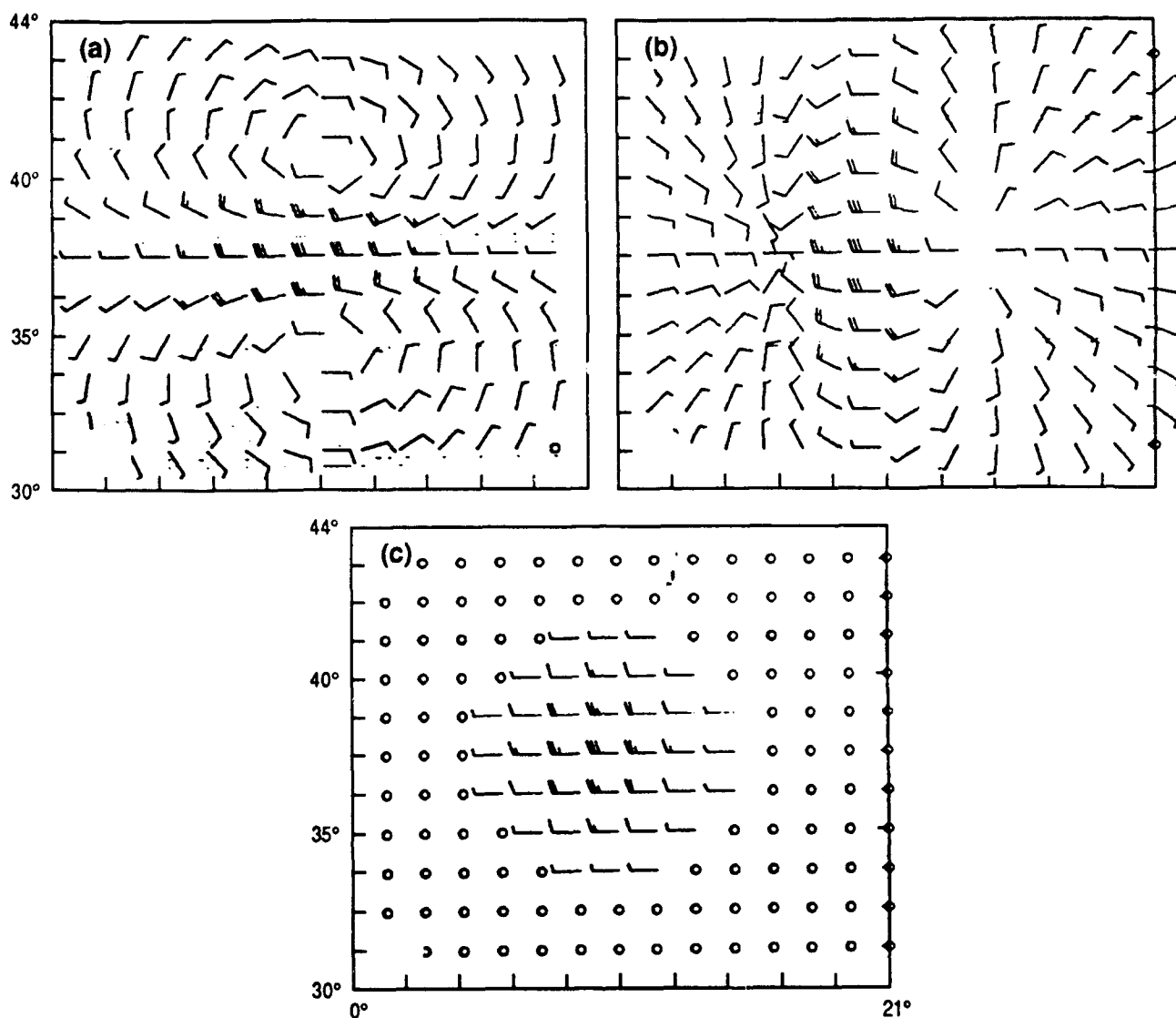


Figure 3. Wind analysis using a single wind value. The divergence parameters was set for (a) fully rotational, (b) fully divergent, and (c) a combination of both divergent and rotational.

signal to an environmental measurement, then all of the observations taken by the instrument will have similar errors. The ability of the optimum interpolation to extract gradient information from a system that contains correlated errors is shown in an experiment in which a series of analyses were performed from four observations. The analyses were identical except for the location of the observations, which were positioned closer together in each succeeding analysis. The estimated analysis error in the center of the observation grid was computed. The results of a series of analyses were plotted to show how the estimated error changed with observation spacing. Figure 5 shows the results of two series of analyses, one with random and the other with correlated observation error. The estimated analysis error in the wind is smaller when the height observation errors were correlated than when they were random, illustrating the capability of the analysis to extract gradient information from otherwise poor data. The estimated error in the height

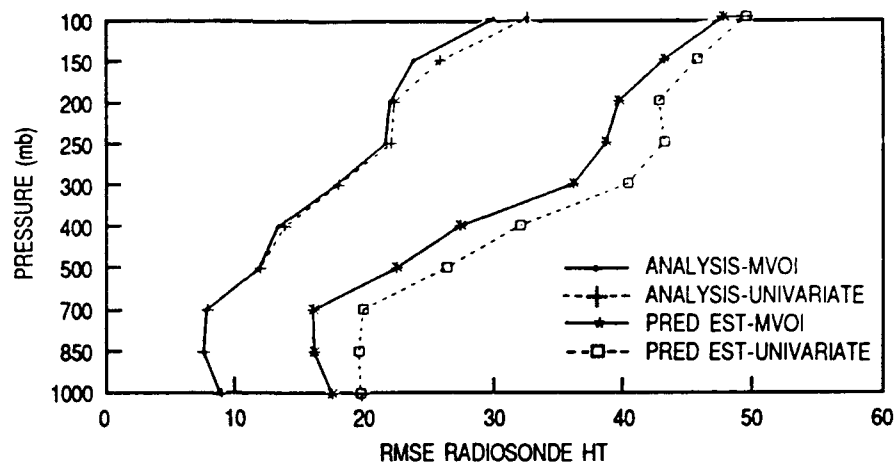


Figure 4. Root-mean-square differences between radiosonde heights and resulting analysis, and between radiosonde heights and the first guess for multivariate analysis and univariate analysis.

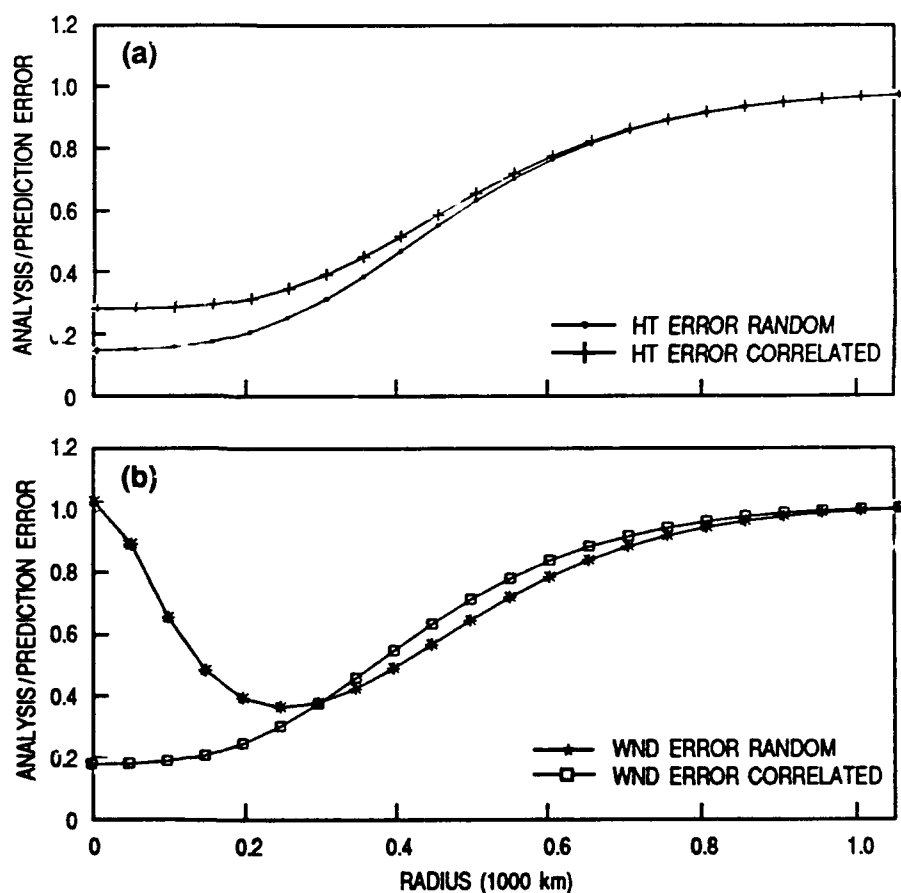


Figure 5. Estimated root-mean-square error in analysis of (a) height and (b) wind, at the center of a four-point observation grid vs. radial distance for four height observations comparing random observation errors with correlated observation errors.

analysis was least when the observational error was random, illustrating that the optimum interpolation is able to remove random error by averaging

the data values, and this capability is improved with observation density. From the viewpoint of utilizing satellite data, increased observation density improves the height analysis when the errors are random, and improves the wind analysis when they are correlated.

Wind observations alone may not produce an accurate height analysis because winds can only contribute to the gradients. This was shown using the method described above except that the four observations were wind. A second series of analyses were done, but with a height observation added to one of the locations. A comparison of the expected errors in heights for the two observation configurations, Figure 6, shows that although the errors were large when winds alone were used, adding a single height observation dramatically decreased the height errors by as much as 50%.

The advantage of the multivariate analysis was also illustrated by the simulation of an aircraft making observations through the southeast sector of a low pressure system. Three different aircraft sensor configurations were simulated: wind sensor alone, height sensor alone, and a combined wind and height sensor. The simulated observations are shown in Figure 7. The true fields are shown with the analyzed fields in Figures 8 and 9. The wind sensor alone simulation gave a reasonable location for the storm, but it was too weak. The height sensor alone simulation produced a more intense storm in the analysis, but it too was weak, and its location was too far southeast. The combined sensor produced the best results, although it, too, lacked intensity. The fit of the analysis to the simulated observations and to the true field is shown in Figure 10. When verified against the observations, the analysis agreed with height observations when using the height-only sensor, and it agreed with wind observations when using the wind-only sensor. Compared to the true field, however, the wind-only sensor produced least accurate results, followed by the height-only sensor. The combined wind and height sensor produced the most accurate analysis reducing the height analysis from the wind-only sensor by 47% and reducing the height analysis error by 25%.

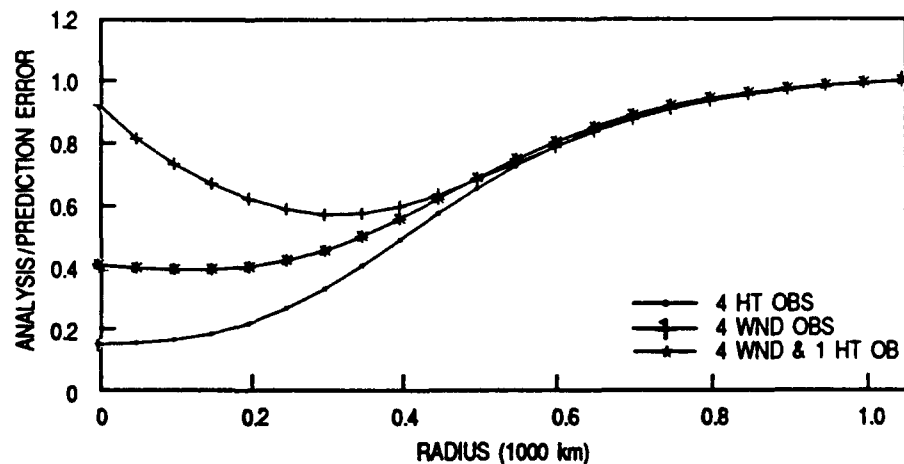


Figure 6. Estimated root-mean-square error in analysis of height at the center of a four-point observation grid vs. radial distance for four height observations, four wind observations, and four wind observations plus one height observation.

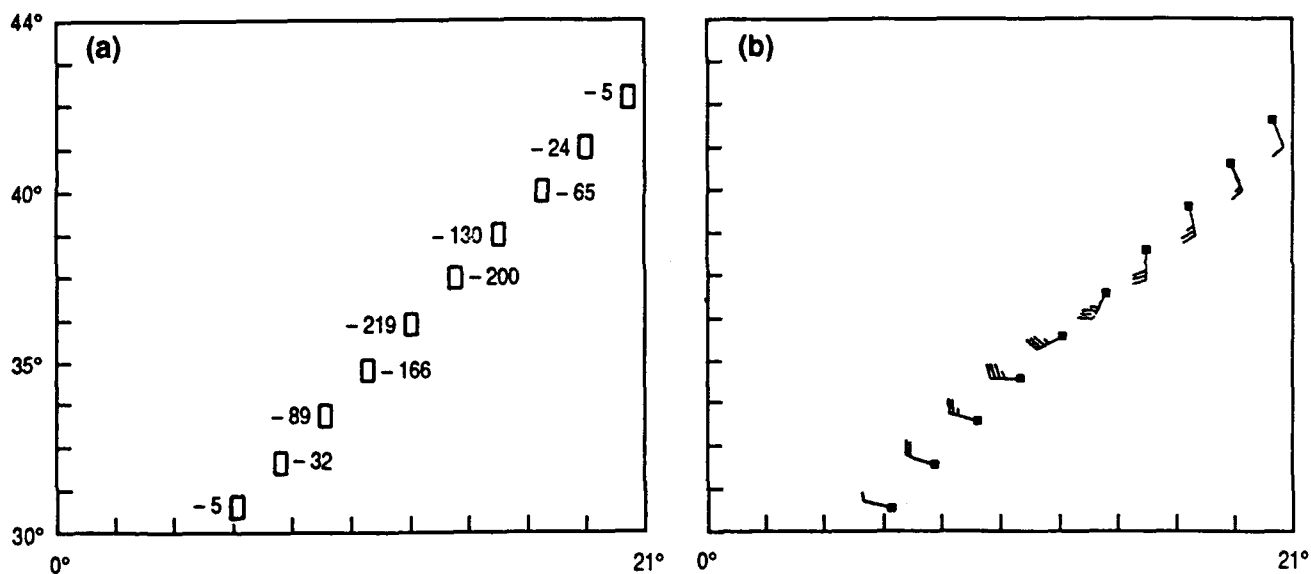


Figure 7. Simulated aircraft observations through the southeast sector of a storm, (a) heights and (b) winds.

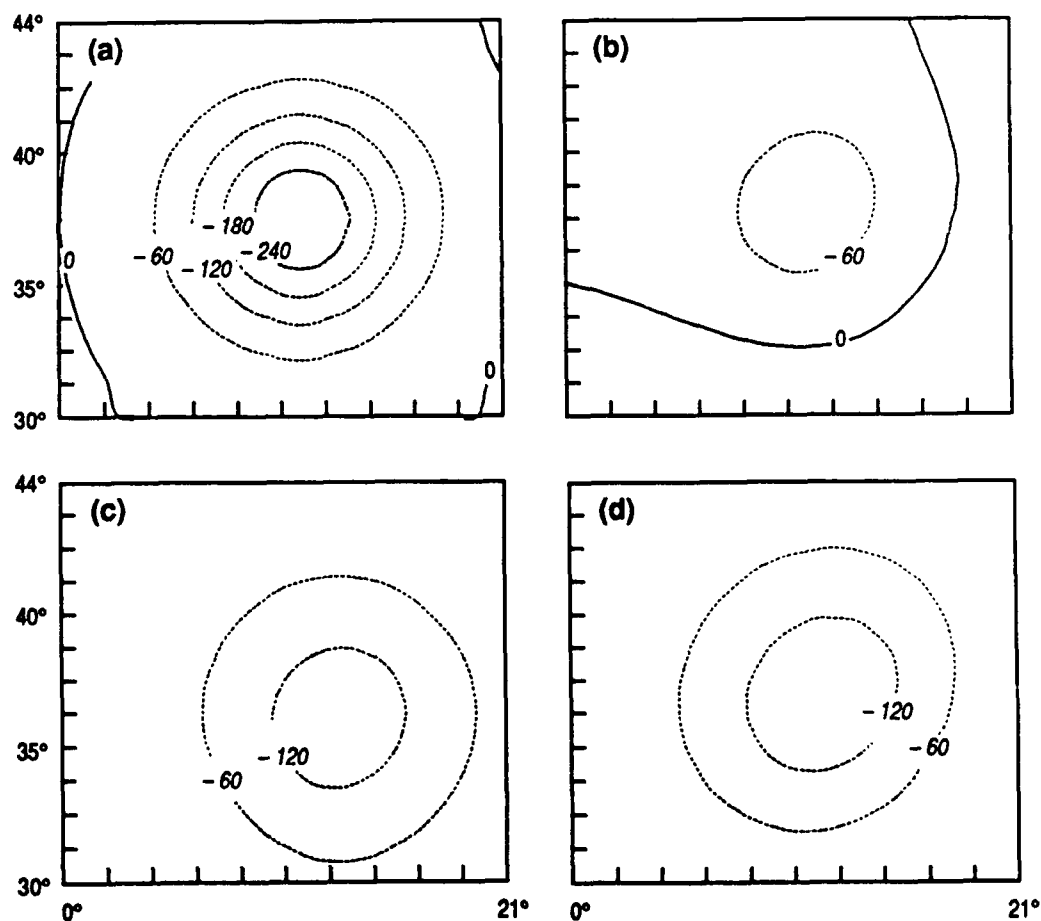


Figure 8. (a) Height pattern of a low pressure system true field, (b) analyzed from a system observing winds alone, (c) analyzed from a system observing heights alone, and (d) analyzed from a system observing winds and heights.

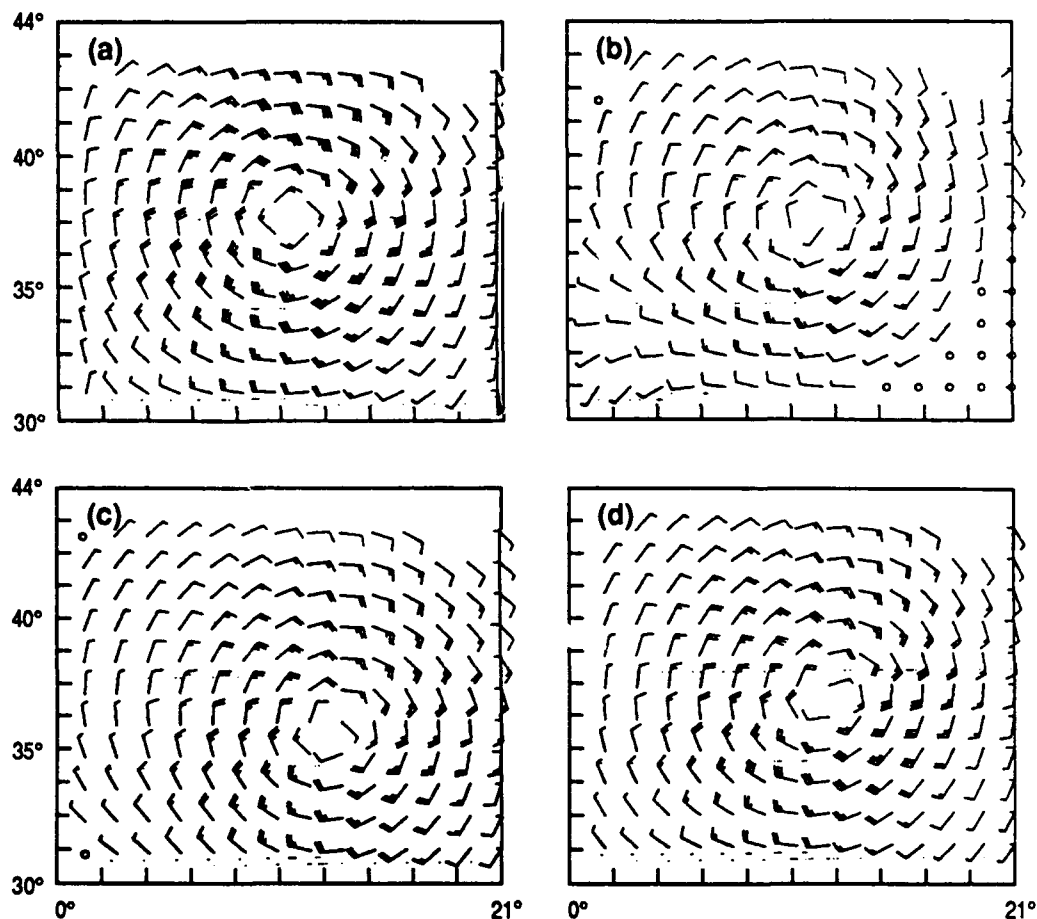


Figure 9. Source as Figure 8 except for winds.

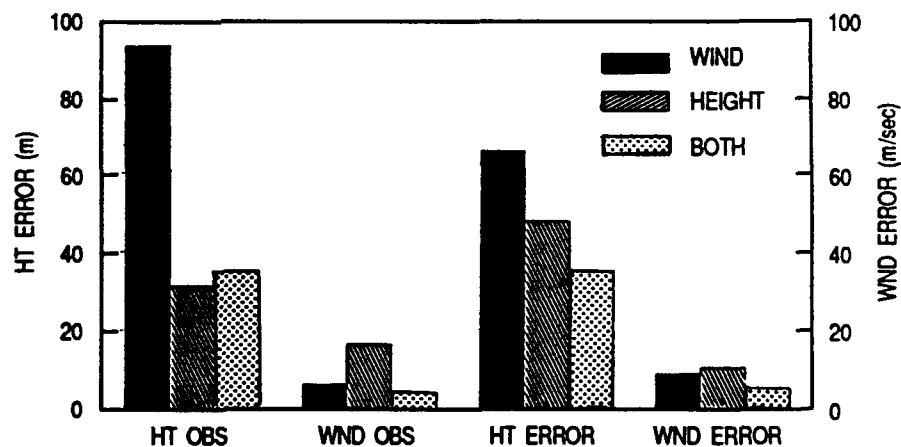


Figure 10. Root-mean-square error as determined from the simulated observations and the true fields. The errors are for three simulations: wind sensor alone, height sensor alone, and combined wind and height sensor. The left half of the graph is for verification against observations and the right half is for verification against the true field.

6.3 Vertical Interpolation

The vertical consistency of the analysis is best maintained with observations of wind and temperature profiles that extend through the analysis layer. To use single level observations such as aircraft

measurements and cloud-track winds requires determination of appropriate vertical covariance function of the prediction error variance. The example illustrated shows how satellite temperature profiles may be combined with single-level observations so that they support each other.

Satellite derived soundings do not contain the reference level needed to convert inferred temperatures to geopotential height, so the observations are given in thicknesses between the standard pressure surfaces. A common method to analyze satellite soundings has been to analyze a reference level, and then convert the satellite derived thicknesses to geopotential heights. Using MVOI, satellite derived thicknesses can be input directly and blended with available reference data.

To test this feature, two analyses were computed. One analysis was given a single thickness observation, and the other was given a thickness and a pressure height observation. To make the results easy to interpret, the observations were assumed to contain no error. After subtracting the predicted estimate, the thickness increment of the 500- to 400-mb layer was -200 m, and the height increment of the 300-mb pressure surface was 0 m. In this test, the horizontal locations of the analysis gridpoints and the observations were horizontally collocated. The vertical covariance model relative to the 500-mb surface is shown in Figure 11. The two analyses and vertical locations for both analyses are shown in Figure 13.

The analysis increment from the single thickness observation produced a 500- to 400-mb layer thickness correction of -200 m. Note that the largest correction occurred at 300 mb. In the second analysis, the 300 mb height observation was added. The analysis increment for the 500- to 400-mb thickness was again -200 m, but this time the analysis increment at 300 mb was 0 m, corresponding to the value of the added observation. In other words, with zero observation error, the analysis *drew* to the observations, in effect using the height observation as a reference level.

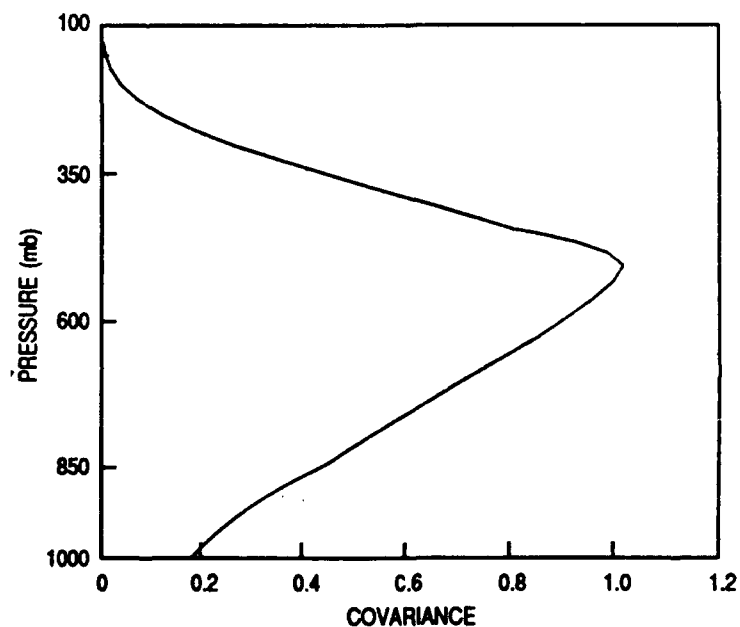


Figure 11. Vertical covariance model relative to 500 mb.

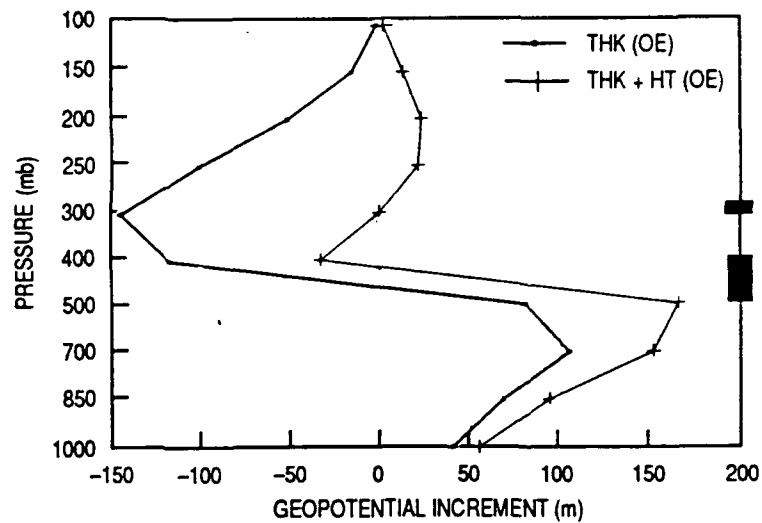


Figure 12. Analysis increment computed from a single thickness observation shown with an analysis increment computed from the single thickness observation and a height observation. Both observations were assumed to contain no error.

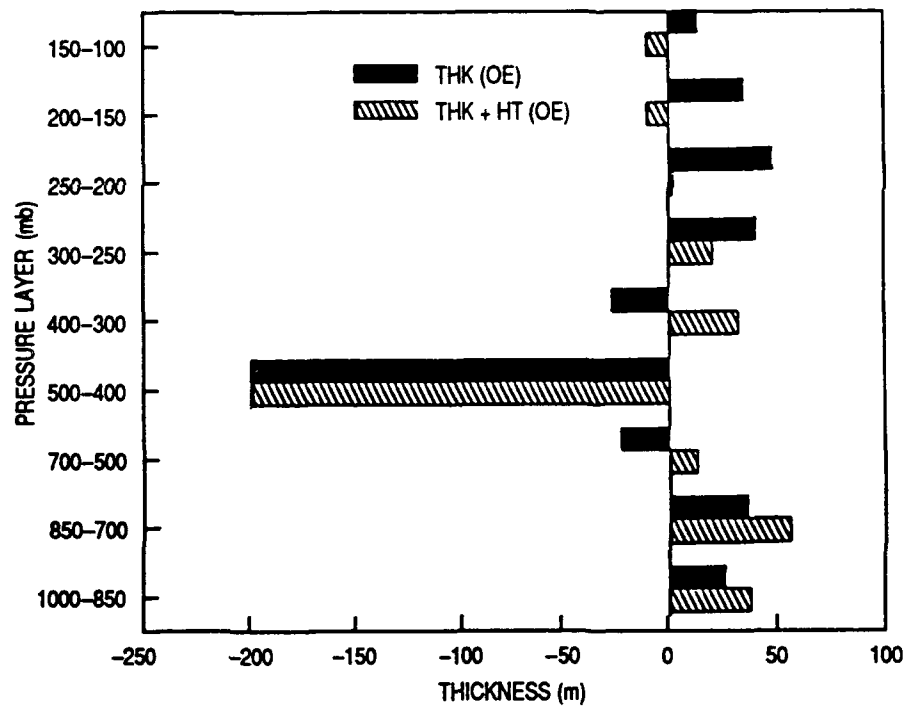


Figure 13. Plots of the thickness of the analyses shown in Figure 12.

In another pair of tests, the observations were assumed to contain random error variance at 80% of the predicted estimate. The analysis increments, shown in Figure 14, were about 45% smaller than the results above, and closer to the increments that would be computed in an actual situation. The analysis did not *draw* exactly to the data, but instead was making a compromise between the predicted estimate and the observations.

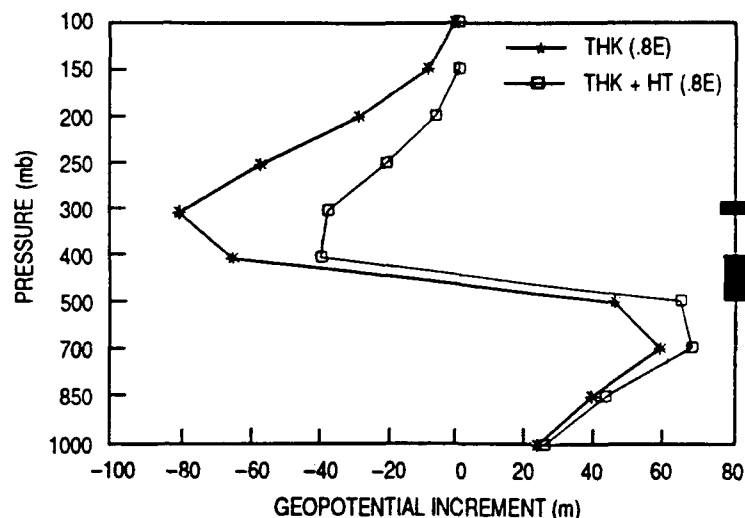


Figure 14. Same as Figure 12 except for observations with errors equal to 80% of the prediction mean error.

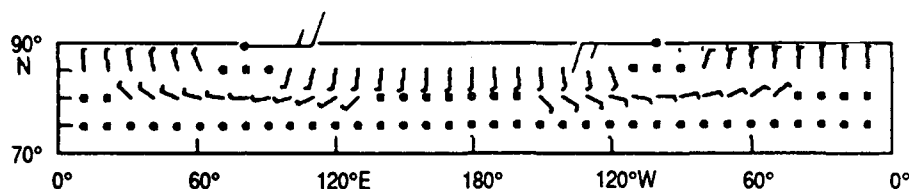


Figure 15. Two wind observations representing the same flow shown plotted on a spherical grid and the resulting analysis.

6.4 Analysis Near Poles

Winds lose their definition of direction on a spherical grid near the poles. To eliminate this problem, the analysis is done with the wind components projected to a polarstereographic projection, and then the product converted back to a spherical grid. The success of this procedure was illustrated by placing two wind observations near the north pole. Although they represent the same flow, projected onto a spherical grid, they appear to flow in opposite directions. The analysis shown in both spherical projection, Figure 15, and polarstereographic projection, Figure 16, agree with the input observation. Tests of the geostrophic constraint in the polar volume across the pole gave results as accurate as other areas.

7.0 Data Selection Procedures

The volume method of MVOI pertains to the procedures used to select observations for analysis at a particular gridpoint. Historically, observations were selected for individual gridpoints, but limited computer time and the belief that five observations containing height and wind would be sufficient to acquire the necessary accuracy kept the typically selected number of observations small. As the computer power increased, most centers increased the number of observations used to analyze a single gridpoint, and the increased numbers surprisingly improved the analysis.

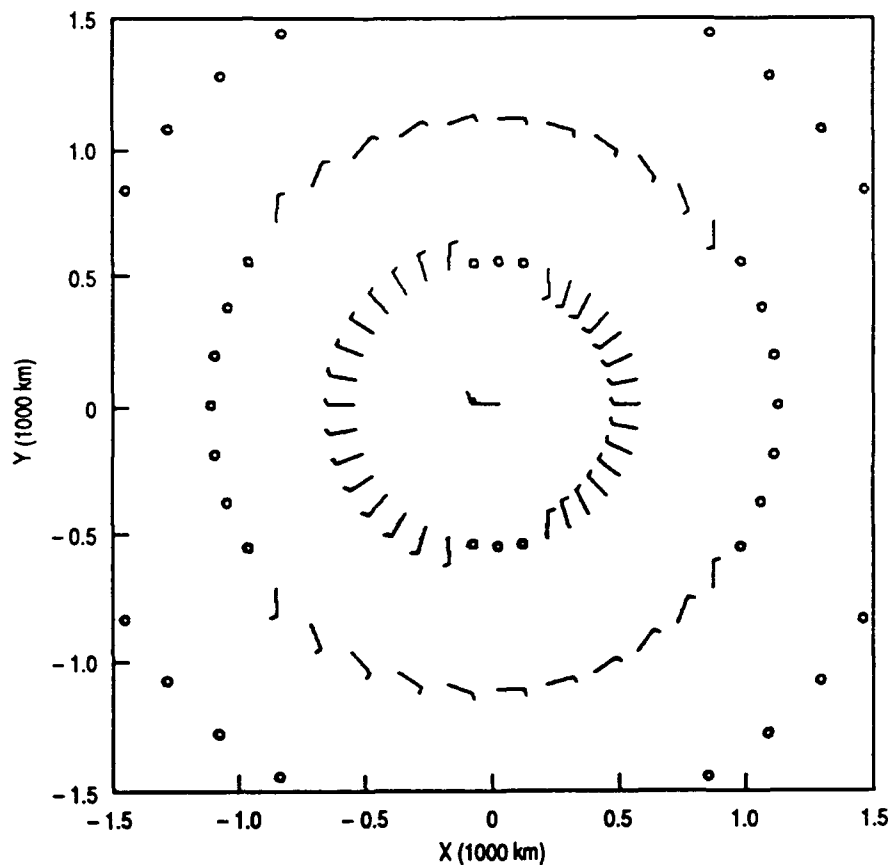


Figure 16. Same as Figure 15 except plotted on a polarstereographic grid.

Lorenc's (1981) solution to using large numbers of observation per gridpoint is to make the selection for volumes of gridpoints. This lessens the computational work load since equation (73) needs to be solved only once for volumes containing from 1,000 to 40,000 points.

The results in section 6 show how a discontinuity can occur in an analysis. Since there is limit to the density of gridpoints one may choose, the solution to the analysis equations for a particular set of observations and error functions is actually a smoothly varying surface. When the observations, functions, or both are changed from one area to the next, the analysis surfaces may take on the appearance of Figure 2, in contrast to Figure 1, where the error functions and observations are the same throughout. Dynamic consistency of the analysis is best obtained using the volume method, because it tends to fit the observations as well as the gridpoint method, plus it is smoother. Obviously, the gridpoint method converges to the volume method as the observation selection and error functions become similar.

With these characteristics in mind, the data selection scheme was designed to achieve several goals:

1. Achieve vertical and horizontal smoothness,
2. Maximize analysis volumes over the polar regions where gridpoint density is largest,
3. Maximize the influence of radiosondes below 100 mb,
4. Maximize the influence of satellite soundings above 100 mb,

5. Maximize the distribution of observations used in the analysis,
6. Minimize computations,
7. Utilize as many of the observations as feasible.

The characteristics of the resultant configuration of observation selection are the following:

1. Analyze over the largest possible polar volume that contains 300 data values, which produced a polar volume that included all gridpoints poleward of $\pm 70^\circ$.

2. Spatially vary observation selection volumes to utilize most observations within a region. This tactic produced volumes over continents that were half as large as the volumes over the oceans of the Southern Hemisphere.

3. Profile observations such as radiosondes, satellite soundings, and PIBALS were either wholly selected or completely excluded, according to a priority list for observation selections instead of arbitrarily selecting values from all profiles. This was done to insure vertical consistency and smoothness.

4. The priority list of observation selection starts with radiosondes and surface observations, and then works through satellite derived thicknesses, PIBAL winds, AIREPs, and finally satellite winds.

5. To get the selected observations to be evenly distributed over the volume, the observations were first sorted by latitude. The selection strategy involves choosing every fourth observation or so starting with the first observation the first time through, the second observation the second time through, etc.

8.0 Internal Quality Control

The strategy for removing observations with errors is not easy, yet the quality of a forecast may fully depend on a correct decision in data quality control. The difficulty can be illustrated using the simulated aircraft scenario of section 6.2 as plotted in Figure 17. In this illustration,

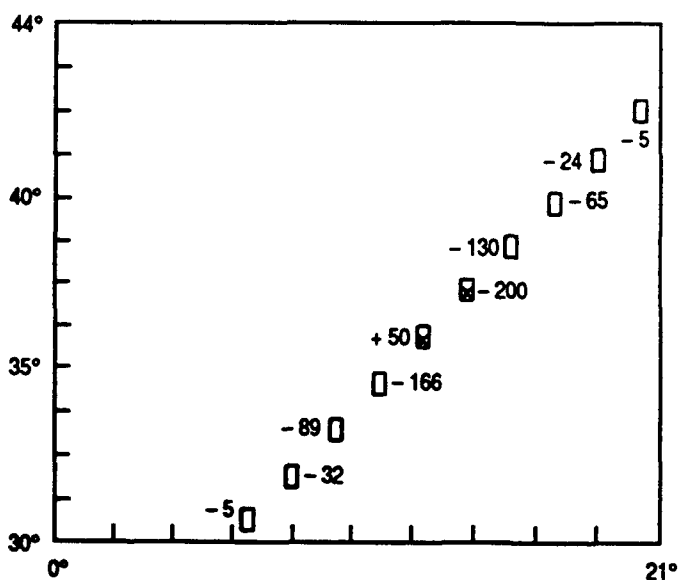


Figure 17. Same as Figure 7a, but for one observation in error. The observations rejected by the analysis are marked by an x.

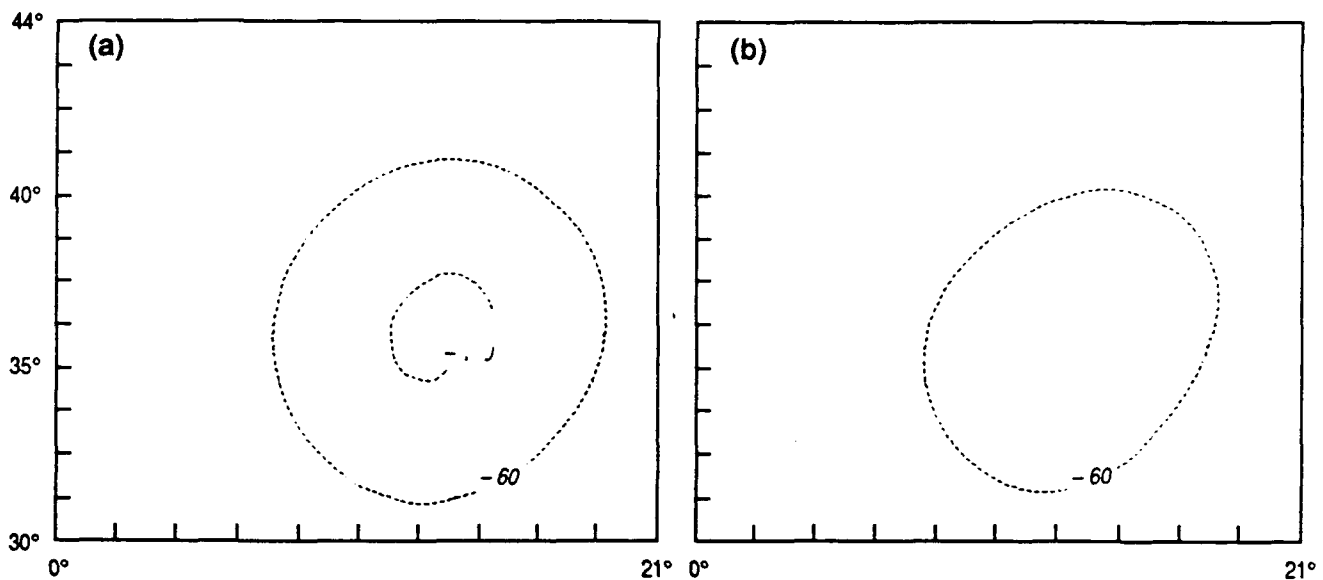


Figure 18. The analysis of height using the observations shown in Figure 17 (a) when only the erroneous observation (reported as +50 m) was marked suspicious and (b) when the erroneous observation and its two closest neighbors were marked suspicious.

the aircraft had a height-only sensor, but one of the observations came in as +50 m instead of -219 m. Two strategies were used to remove the error. In one instance, only the erroneous observation was marked suspicious, and in the other the erroneous observation and the observations on either side were marked suspicious. The solutions for the two cases were completely different (Fig. 18). When only the observation in error was marked suspicious, it was correctly eliminated, but when the erroneous observation and its two nearest neighbors were marked suspicious, a key observation was eliminated. The eliminated observations are shown in Figure 17 marked by an "x" for the test where more than the erroneous observations were marked suspicious.

Clearly, the problem illustrated here is the result of a sparsely observed region. But it is this sparsity that makes the quality control solution so critical. It is recognized that as much preprocessing as possible be utilized, and that the internal quality control be given as much assistance as possible to make the correct decisions.

There are many other things that can be done to insure that only the highest quality observations get into the analysis, and the process is continually evolving.

For example, work is ongoing to utilize the performance history of the observations and to eliminate consistently bad stations (see Baker et al., 1991).

9.0 Conclusions

Although there are newer and better methods being developed, there are still things that can be done to make the Navy MVOI give better results. Suggestions based on the experience gained since the system became operational in 1988 are presented below.

The MVOI couples the wind and geopotential linearly using the geostrophic relationship. It has been shown by Williamson and Daley

(1983) that the model rejects some of the information provided by the observations. Some of this rejection may be caused from application of linear analysis methods to the nonlinear atmosphere. An iterative-analysis-initialization procedure has been shown to solve this problem through making the corrections to the model nonlinear. This could be applied to the existing system without much redesign, and some studies using a shallow-water version of the NOGAPS data assimilation system are being conducted.

Even though the analysis method is capable of analyzing for the divergent component of the wind field, this divergent flow gets rejected by the data assimilation system, and consequently is removed by the nonlinear normal mode initialization. Studies are needed to couple the analysis of divergence with moisture in the tropics (Krishnamirti et al., 1988), which will force the model to more closely simulate the tropical divergence associated with cumulus clouds.

The tight coupling of the tropics and the midlatitudes make the tropical analysis and initialization more important. This has been demonstrated by Gelaro (1991) and the time scales for interaction between the tropics and midlatitudes is well within the range of predictability expected from NOGAPS.

More intelligence is required to insure the best observational information is input to the data analysis. The early work of Baker et al. (1991) may evolve into artificially intelligent data selection software that tests the recent performance of observations, the atmosphere's instabilities, and model performance before deciding on the appropriate data to use.

The prediction errors are known to vary, particularly where the atmosphere is baroclinically and convectively unstable. New methods are being developed to improve estimates of predication errors.

Much more work is still required to improve the range and accuracy of NOGAPS. The importance of data quality control, data analysis, and data rejection in the model require that attention be directed toward prediction system improvement.

10.0 References

1. Baker, N. (1991a). An adaptive correction procedure for radiosonde geopotential height biases. Presented at *Ninth Conference on Numerical Weather Prediction*, Denver, CO, October 1991.
2. Baker, N. (1991b). Quality control for the FNOC operational atmospheric database. Naval Oceanographic and Atmospheric Research Laboratory, Stennis Space Center, MS, NOARL Report 25.
3. Baker, N. (1991). Quality control of meteorological observations. Naval Oceanographic and Atmospheric Research Laboratory, Stennis Space Center, MS, NOARL Report 26.
4. Baker, N. (1992). Data quality control for the Naval Operational Global Atmospheric Prediction System. *Weather and Forecasting*, 7:250-261.
5. Barker, E. H. and T. E. Rosmond (1985). Short course on objective data analysis and vector computers. *Bulletin of the American Meteorological Society* 66: 1153-1161.

6. Barker, E., J. Goerss, and N. Baker (1988). The Navy's operational multivariate optimum interpolation analysis method. Presented at *Eighth Conference on Numerical Weather Prediction*, Baltimore, MD.
7. Barker, E. (1992). Design of the Navy's multivariate optimum interpolation analysis system. *Weather and Forecasting*, 7:220-231.
8. Bengtsson (1976). Initial data and some practical aspects of weather forecasting. *Weather Forecasting and Weather Forecasts: Models, Systems, and Users - Volume 1*. NCAR notes from a Colloquium. Murphy and Williamson, eds., NCAR/CQ-5+1976-ASP, 254-419.
9. Bergman, K. H. (1976). Multivariate objective analysis of temperature and wind fields using the thermal wind relationship. Presented at *Sixth Conference on Weather Forecasting and Analysis*, Albany, NY, May 10-13.
10. Bergman, K. H. (1979). Multivariate analysis of temperatures and winds using optimum interpolation. *Monthly Weather Review* 107: 1423-1444.
11. Daley, R. (1985). The analysis of synoptic scale divergence by a statistical interpolation procedure. *Monthly Weather Review* 113: 1066-1079.
12. Daley, R. (1991). *Atmospheric Data Analysis*. Cambridge University Press, 457 pp.
13. Franke, R. (1984). Sources of error in objective analysis. Naval Postgraduate School, Tech. Report NPS-5-3-003, Monterey, CA, 50 pp.
14. Franke, R. (1986). Covariance functions for statistical interpolation. Naval Postgraduate School, Tech. Report NPS-53-86-007, Monterey, CA, 80 pp.
15. Franke, R., E. Barker, and J. Goerss (1988). The use of observed data for the initial-value problem in numerical weather prediction. *Computational Mathematics Applications* 16: 169-184.
16. Gandin, L. S. (1963). *Objective Analysis of Meteorological Fields*, Translated from Russian by Israel Program for Scientific Translations, 1965, NTIS No. TT 65-50 007, 242 pp.
17. Goerss, J. S. and P. A. Phoebus (1992). The Navy's atmospheric analysis. *Weather and Forecasting*, 7:232-249.
18. Gelaro, R. (1990). The structure and dynamics of tropical-midlatitude interactions. Naval Oceanographic and Atmospheric Research Laboratory, Stennis Space Center, MS, NOARL Report 7.
19. Hogan, T. F. and T. E. Rosmond (1991). The description of the Navy Operational Global Atmospheric Prediction System's Spectral Forecast Model. *Monthly Weather Review* 119: 1786-1815.
20. Krishnamirti, T., H. Bedi, W. Heckley, and K. Ingles (1988). On the reduction of spin up time for evaporation and precipitation in a global spectral model. *Monthly Weather Review* 116: 907-920.
21. Lorenc, A., I. Rutherford, and G. Larsen (1977). The ECMWF analysis and data-assimilation scheme: analysis of mass and wind fields. European Centre for Medium-Range Weather Forecasts, Tech. Report No. 6.
22. Lorenc, A. C. (1981). A global three-dimension multivariate statistical interpolation scheme. *Monthly Weather Review* 109: 701-721.

23. Meyers (1986). Can software for the Strategic Defense Initiative ever be error-free? *IEEE-Computer*, p. 61-67.
24. McPherson, R. D., K. H. Bergman, R. E. Kistler, G. E. Rasch, and D. S. Gordon (1979). The NMC operational global data assimilation system. *Monthly Weather Review* 107: 1445-1461.
25. Parnas (1985). Software aspects of strategic defense systems. *American Science* 73: 432-440.
26. Rosmond, T. E. (1992). The Design and Testing of the Navy Operational Global Atmospheric Prediction System. *Weather and Forecasting*, 7:262-272.
27. Rutherford, I. D. (1976). An operational three-dimensional multivariate statistical objective analysis scheme. Presented at *Proceedings of the JOC Study Group Conference on Four-Dimensional Data Assimilation*, Paris, November 17-21, GARP Report No. 11.
28. Rutherford, I. D. (1978). An operational three-dimensional multivariate statistical objective analysis scheme. Notes Scientifiques et Techniques, 1, Division de Recherche en Prevision Numerique, Montreal, Canada.
29. Schlatter, T. W. (1975). Some experiments with a multivariate statistical objective analysis scheme. *Monthly Weather Review* 103: 246-257.
30. Williamson, D. L. and R. Daley (1983). A unified analysis initialization technique. *Monthly Weather Review* 111: 1517-1536.

Distribution List

Applied Physics Laboratory
Johns Hopkins University
Johns Hopkins Road
Laurel MD 20707

Applied Physics Laboratory
University of Washington
1013 NE 40th St.
Seattle WA 98105

Applied Research Laboratory
Pennsylvania State University
P.O. Box 30
State College PA 16801-0030

Applied Research Laboratory
University of Texas at Austin
P.O. Box 8029
Austin TX 78713-8029

Assistant Secretary of the Navy
Research, Development & Acquisition
Navy Department
Washington DC 20350-1000

Chief of Naval Operations
Department of the Navy
Washington DC 20350-2000
Attn: OP-71
OP-987

Chief of Naval Operations
Oceanographer of the Navy
U.S. Naval Observatory
34th & Massachusetts Ave. NW
Washington DC 20392-1800
Attn: OP-096
OP-096B

Defense Mapping Agency
8613 Lee Hwy.
Fairfax VA 22031-2138
Attn: Code PRN, Mailstop A-13
Director

Fleet Antisub Warfare Tng Ctr-Atl
Naval Station
Norfolk VA 23511-6495
Attn: Commanding Officer

Fleet Numerical Oceanography Center
Monterey CA 93943-5005
Attn: Commanding Officer

National Ocean Data Center
1825 Connecticut Ave., NW
Universal Bldg. South, Rm. 206
Washington DC 20235

Naval Air Systems Command HQ
Washington DC 20361-0001
Attn: Commander

Naval Air Warfare Center
Aircraft Division Warminster
Warminster PA 18974-5000
Attn: Commander

Naval Civil Engineering Laboratory
Port Hueneme CA 93043
Attn: Commanding Officer

Naval Command Control and Ocean
Surveillance Center
RDT&E Division
San Diego CA 92152-5000
Attn: Commander

Naval Facilities Engineering Command
200 Stovall St.
Alexandria VA 22332-2300
Attn: Commander

Naval Oceanographic Office
Stennis Space Center MS 39522-5001
Attn: Commanding Officer
Code TD
Library (2)

Naval Oceanography Command
Stennis Space Center MS 39529-5000
Attn: Commander

Naval Postgraduate School
Monterey CA 93943
Attn: Superintendent

Naval Research Laboratory
Atmospheric Directorate
Monterey CA 93943-5006
Attn: Director
Code 400

Naval Research Laboratory
Stennis Space Center MS 39529-5004
Attn: Code 115
Code 125L (10)
Code 125P
Code 200
Code 300

Naval Research Laboratory
Washington DC 20375-5320
Attn: Commanding Officer
Library (2)

Naval Sea Systems Command HQ
Washington DC 20362-5101
Attn: Commander

Naval Surface Warfare Center
Dahlgren Division
Detachment White Oak
10901 New Hampshire Ave.
Silver Spring MD 20903-5000
Attn: Officer in Charge
Library

Naval Surface Warfare Center
Dahlgren Division
Dahlgren VA 22448-5000
Attn: Commander

Naval Surface Warfare Center
Coastal Systems Station
Dahlgren Division
Panama City FL 32407-5000
Attn: Commanding Officer

Naval Surface Warfare Center
Carderock Division
Bethesda MD 20084-5000
Attn: Commander

Naval Undersea Warfare Center
Division
Newport RI 02841-5047
Attn: Commander

Naval Undersea Warfare Center Det
New London CT 06320
Attn: Officer in Charge

Office of Naval Research
800 N. Quincy St.
Arlington VA 22217-5000
Attn: Code 10D/10P, E. Silva
Code 112, E. Hartwig
Code 12
Code 10

Office of Naval Research
ONR European Office
PSC 802 Box 39
FPO AE 09499-0700
Attn: Commanding Officer

Office of Naval Technology
800 N. Quincy St.
Arlington VA 22217-5000
Attn: Code 20, P. Selwyn
Code 228, M. Briscoe
Code 228, CDR L. Bounds
Code 22, T. Warfield

Scripps Institution of Oceanography
University of California
291 Rosecrans St.
San Diego CA 92106-3505

Scripps Institution of Oceanography
P.O. Box 6049
San Diego CA 92166-6049

Space & Naval Warfare Sys Com
Director of Navy Laboratories
SPAWAR 005
Washington DC 20363-5100
Attn: Commander

Woods Hole Oceanographic Institution
P.O. Box 32
Woods Hole MA 02543
Attn: Director

REPORT DOCUMENTATION PAGE

Form Approved
OMB No. 0704-0188

Public reporting burden for this collection of information is estimated to average 1 hour per response, including the time for reviewing instructions, searching existing data sources, gathering and maintaining the data needed, and completing and reviewing the collection of information. Send comments regarding this burden estimate or any other aspect of this collection of information, including suggestions for reducing this burden, to Washington Headquarters Services, Directorate for Information Operations and Reports, 1215 Jefferson Davis Highway, Suite 1204, Arlington, VA 22202-4302, and to the Office of Management and Budget, Paperwork Reduction Project (0704-0188), Washington, DC 20503.

1. Agency Use Only (Leave blank).		2. Report Date. July 1992		3. Report Type and Dates Covered. Final	
4. Title and Subtitle. The Development of the Navy's Multivariate Optimum Interpolation Analysis System				5. Funding Numbers. Job Order No. 94312D Program Element No. 0603207N Project No. Task No. Accession No.	
6. Author(s). E. H. Barker					
7. Performing Organization Name(s) and Address(es). Naval Oceanographic and Atmospheric Research Laboratory Atmospheric Directorate Monterey, California 93943-5006				8. Performing Organization Report Number. NOARL Report 44	
9. Sponsoring/Monitoring Agency Name(s) and Address(es).				10. Sponsoring/Monitoring Agency Report Number.	
11. Supplementary Notes.					
12a. Distribution/Availability Statement. Approved for public release; distribution is unlimited. Naval Oceanographic and Atmospheric Research Laboratory, Stennis Space Center, Mississippi 39529-5004.				12b. Distribution Code.	
13. Abstract (Maximum 200 words). The equations for the Navy's multivariate optimum interpolation (MVOI) analysis system for atmospheric analysis are presented in complete form. Included are the derivations for horizontal and vertical covariances that retain the geostrophic constraint and blend various kinds of observations such as pressure thickness, pressure height, and winds. Methods that scale the observation values to the resulting nondimensional values so that they are consistent with the constraints are presented. The derivations of the analysis equations are provided using optimal theory to minimize the analysis error variance. The derivation of the internal data checking procedure is given. The method compares suspicious values with neighboring values and removes rejected values in a computationally consistent manner. Validation experiments that show the exactness of the constraints, expected analysis error, and the method for analysis of wind around the poles are presented. These experiments have known results, and therefore are useful in catching design and program errors. A brief description is provided of the observation selection procedures and internal quality control, and some recommendations for improvement are given.					
14. Subject Terms.				15. Number of Pages. 37	
				16. Price Code.	
17. Security Classification of Report. Unclassified	18. Security Classification of This Page. Unclassified	19. Security Classification of Abstract. Unclassified	20. Limitation of Abstract. None		